Geodinamica Acta
Publication details, including instructions for authors and subscription information:
http://www.tandfonline.com/loi/tgda20

Tectono-metamorphic history of the ophiolitic Lento unit (northern Corsica): evidences for the complexity of accretion-exhumation processes in a fossil subduction system

Nicola Levi [a] , Alessandro Malasoma [b] , Michele Marroni [b a] , Luca Pandolfi [b a] & Matteo Paperini [b]
[a] Istituto di Geoscienze e Georisorse , CNR , Pisa , Italy
[b] Dipartimento di Scienze della Terra , Università di Pisa , Via S. Maria, 53, 56126 , Pisa , Italy
Published online: 13 Apr 2012.

To cite this article: Nicola Levi , Alessandro Malasoma , Michele Marroni , Luca Pandolfi & Matteo Paperini (2007) Tectono-metamorphic history of the ophiolitic Lento unit (northern Corsica): evidences for the complexity of accretion-exhumation processes in a fossil subduction system, Geodinamica Acta, 20:1-2, 99-118

To link to this article: http://dx.doi.org/10.3166/ga.20.99-118

Geodinamica Acta 20/1-2 (2007) 99-118

Geodinamica Acta

Tectono-metamorphic history of the ophiolitic Lento unit (northern Corsica): evidences for the complexity of accretion-exhumation processes in a fossil subduction system

Nicola Levi [1], Alessandro Malasoma [2], Michele Marroni [2,1*], Luca Pandolfi [2,1], Matteo Paperini [2]

[1] *Istituto di Geoscienze e Georisorse, CNR, Pisa, Italy*

[2] *Dipartimento di Scienze della Terra, Università di Pisa, Via S. Maria, 53 56126 Pisa Italy*

Received: 30/01/06, accepted: 01/10/06

Abstract

The Alpine Corsica (Corsica Island, France) is characterized by a stack of continent- and ocean-derived tectonic units, known as Schistes Lustrés complex. This complex is affected by deformation and metamorphic imprint achieved during Late Cretaceous – Early Tertiary subduction-related processes connected with the closure of the Ligure-Piemontese oceanic basin and subsequent continental collision.

In the Schistes Lustrés complex, the Lento oceanic unit is characterized by four deformation phases, from D1 to D4 phase.

The D1 phase, characterized by blueschist metamorphism, is regarded as related to coherent underplating in a subduction zone at a depth of about 25-30 km. The subsequent deformation phases can be referred to exhumation history, as suggested by the continuous decrease of metamorphic conditions. The transition from accretion to exhumation is represented by the D2 phase, achieved during the development of a duplex structure of accreted units. The D3 phase is in turn achieved by a further horizontal shortening, whereas the D4 phase is developed during an extensional event representing the final exhumation of the Lento unit.

On the whole, the data collected for the Lento unit suggest an history that include an accretion by coherent underplating followed by exhumation, more complex than previous described.

Keywords: ophiolites, Lento unit, subduction, accretion, exhumation, Corsica Island

1. Introduction

Most of the modern convergent margins are characterized by the development of an accretionary wedge, i.e. a lithospheric-scale structure located at the boundary between the upper and lower plate. In the accretionary wedge most of the deformation processes connected to the growth of the continental lithosphere occur. The development of an accretionary wedge occurs by a mechanism referred as accretion, consisting in the transfer to the wedge of slices made up of deformed oceanic lithosphere detached from the lower plate. Generally, the accretion occurs after the underthrusting of the oceanic lithosphere to various depth along the subduction plane. After its accretion, the material is generally affected by progressive exhumation up to the exposure at the surface. Modern accretionary complexes (Barbados, Nankai, etc..) have

* Corresponding author.
E-mail address: marroni@dst.unipi.it

doi:10.3166/ga.20.99-118

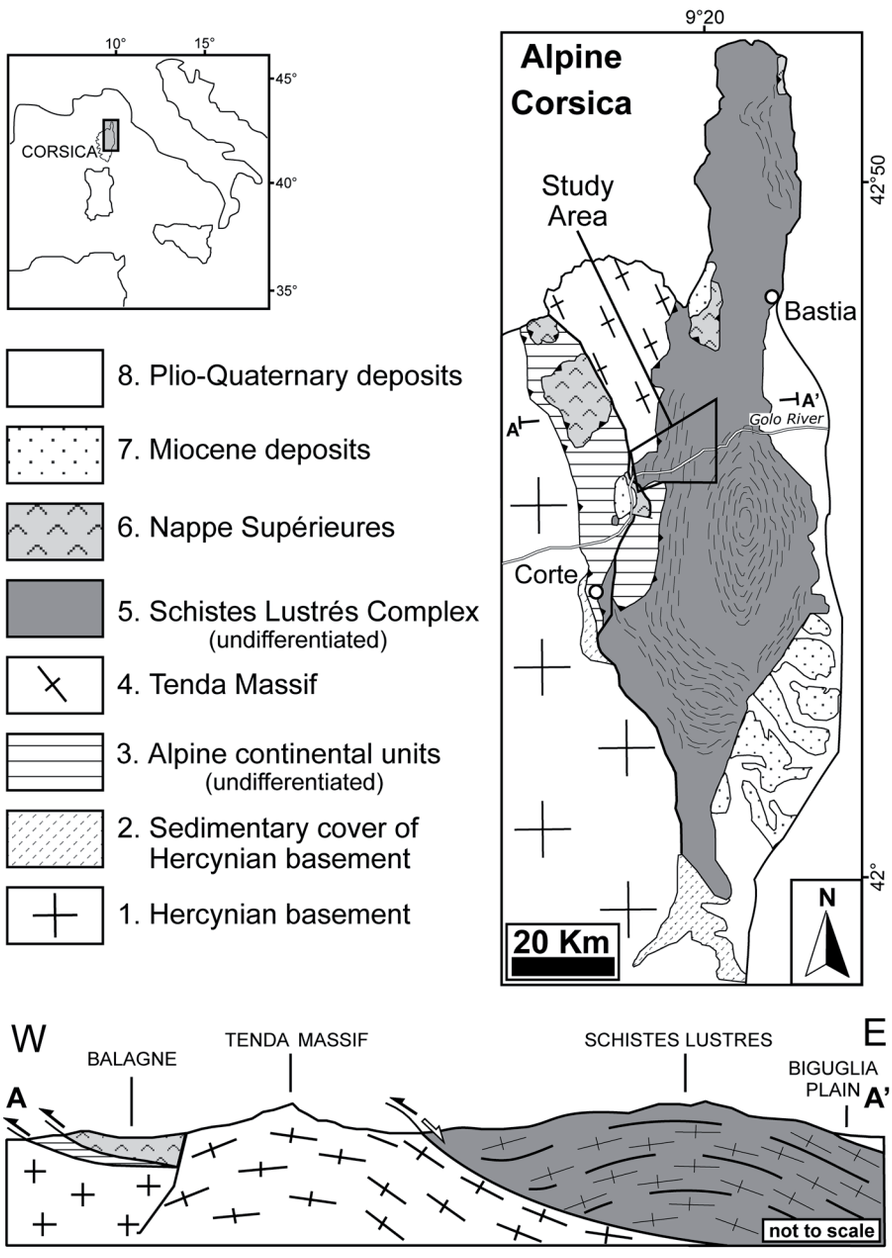

Fig. 1: Tectonic sketch map of Alpine Corsica.

been investigated, mainly by geophysical studies. However, these studies are unable to provide a comprehensive view of the accretion-exhumation mechanisms, because they can not provide detailed observations of the deep structural level of accretion. Valuable informations can be provided by structural studies of fossil oceanic units preserved into collisional belts. However, most of these units record accretion at depth (>30-40 km) and generally show very complex deformation history, where the first stages of the exhumation are generally transposed by later deformations. By contrast, the tectonic units that have suffered accretion at moderate depth (from 20 to 30 km) generally provide all the elements for a complete reconstruction of their history, from accretion up to their exposure at the surfaces.

In the Schistes Lustrés complex, Alpine Corsica, the Lento oceanic unit is characterized by a well exposed succession with a blueschist facies metamorphic overprint. In this unit, the accretion and post-accretion deformations are still well preserved, thus providing a complete set of elements for the full reconstruction of the tectonic history of the Lento unit.

In this paper, a reconstruction of the deformations related to the transition from accretion to exhumation history of the Lento unit is proposed, and the implications for the active processes in the accretionary wedges are discussed.

2. Geological Framework

The tectonic setting of the Corsica Island is characterized by a complex stack of tectonic units, i.e. the Alpine Corsica, thrust over its foreland, i.e. the Hercynian Corsica (Fig. 1).

The Hercynian Corsica is represented by a basement of Variscan age mainly consisting of Carboniferous-to-Permian granitoids and associated volcanic rocks intruded in Precambrian and Palaeozoic country-rocks [1 and quoted references]. Only in the westernmost area, the Variscan basement is characterized by remnants of a Mesozoic-Late Eocene, mainly siliciclastic sedimentary cover [e.g. 2].

The stack of tectonic units from Alpine Corsica includes both oceanic and continental units, generally characterized by a strong deformation associated with metamorphic signature [e.g. 1, 2, 3, 4, 5, 6, 7, 8, 9, 10]. The oceanic units are considered remnants of the Ligure-Piemontese domain, i.e. part of the western Tethys oceanic basin, developed between the European and Adria continental margins during the Triassic rifting and Jurassic spreading phases. Since "mid" Cretaceous time, the Ligure-Piemontese oceanic basin experienced convergence resulting in the inception of intraoceanic subduction processes. The subduction phase resulted in the development of an accretionary wedge, consisting of a pile of oceanic units showing deformations associated with high-pressure (HP) metamorphism. The intraoceanic subduction was followed by the continental collision, whose inception was represented by the involvement of continental crust slices in the subduction zone, probably during Early Tertiary time. Since Early Oligocene time, the compressional tectonics in Corsica were followed by large-scale extension leading to the collapse of the previously thickened orogenic wedge. During Miocene time, the opening of the Liguro-

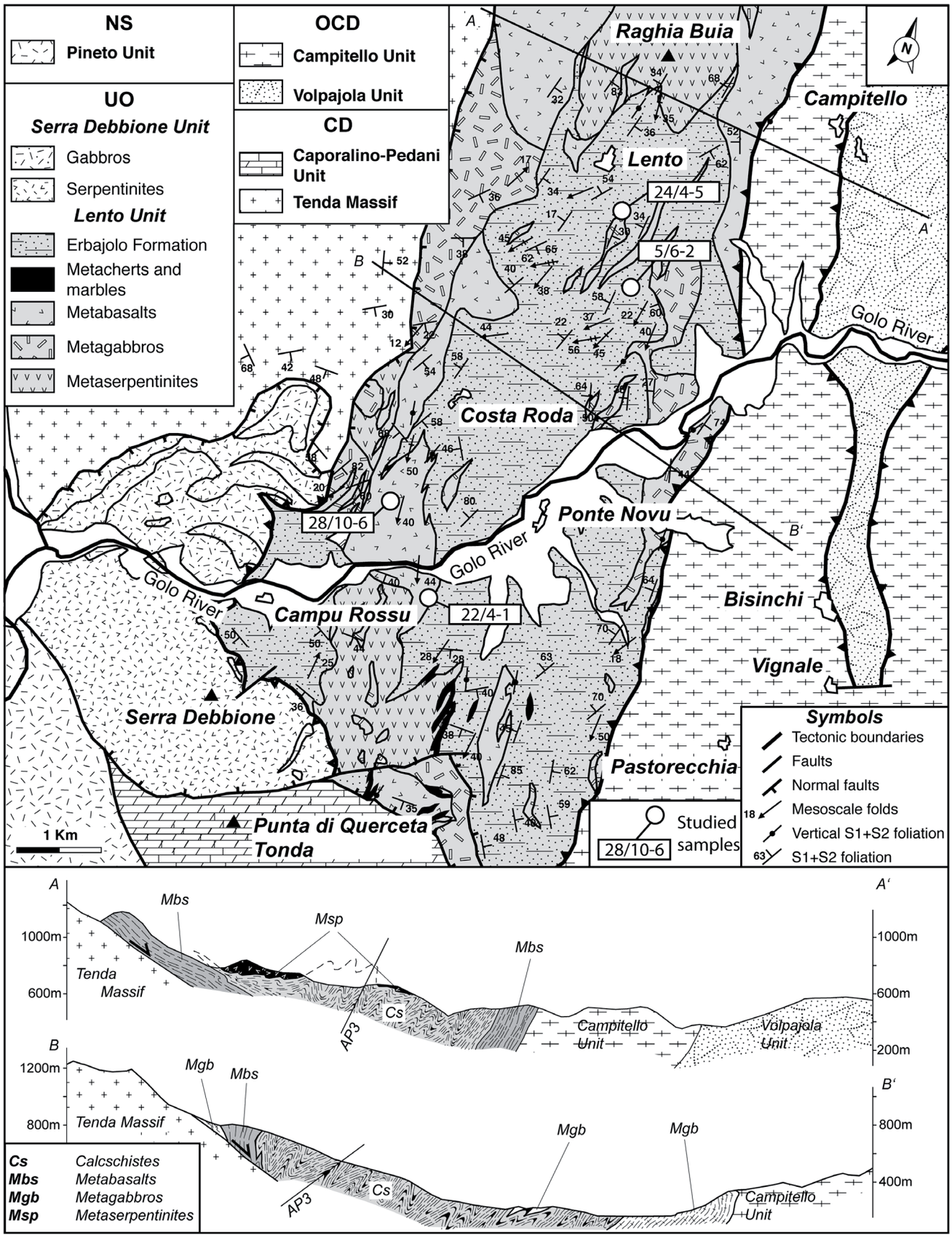

Fig. 2: Geological map of the study area and related geological sections. NS Nappes supérieures; **UO** Upper Ophiolitic units; **OCD** continental- and oceanic-derived units; **CD** continental-derived units.

Provençal and the Thyrrenian basins completely isolated Alpine Corsica from the neighboring collisional belts.

The processes related to the intraoceanic subduction and the subsequent continental collision are well recorded by the dominant deformation and the associated metamorphism observed in the oceanic and continental units belonging to the Schistes Lustrés complex [11, 3, 4, 5, 6, 7, 8, 12, 13, 10]. In this complex, the ophiolite sequences are generally characterized by Late Cretaceous deformations associated to HP/LT metamorphism [14, 15] ranging from low-grade to blueschist and eclogite facies [14, 16, 17, 18]. Also the continental crust displays an HP metamorphism of Early Tertiary age [19 and quoted references]. Both oceanic and continental units are subsequently affected by retrograde metamorphism developed under decreasing pressure in the Middle Eocene to Miocene time span, from 45 to 24 Ma [19]. This metamorphism and the associated deformations are generally referred to exhumation of the Schistes Lustrés complex during the extensional large-scale tectonics developed during the collapse of the previous thickened orogenic belt [12, 13, 18, 20, 19].

The Schistes Lustrés complex overlies a set of continental-derived tectonic units (S.Lucia Nappe, Caporalino-S.Angelo Nappe, Corte units, Annunciata unit and Tenda massif), interpreted as derived from the European plate margin. These units consist of slices of Late Carboniferous-Mesozoic to Middle Eocene sedimentary cover associated with remnants of its crystalline basement. Generally, these units, are characterized by polyphase deformation associated to Alpine metamorphism ranging from very low-grade to blueschist facies conditions [21, 22, 23, 24, 25, 26]. At the top of the Schistes Lustrés, an assemblage of very low-grade metamorphic units (Nappes supérieures) have been recognized as klippen [e.g. 27]. They are mainly represented by ophiolitic units (Balagne and Nebbio units) but slices represented of Late Cretaceous turbidites (Macinaggio and Bas-Ostriconi units) also occur.

The relationships among the Schistes Lustrés, the Nappes supérieures and the continental-derived units are sealed by the Miocene (Burdigalian-Langhian) sedimentary deposits cropping out in the S.Florent and Francardo areas.

3. Geology of the Golo Valley

The study area is located in the middle part of the Golo Valley, an E-W trending, deep canyon where the large scale structure of the Schistes Lustrés complex can be fully observed. This structure is represented by a pile of tectonic units deformed into a large scale N-S trending antiform with steep axial plane. This structure is bounded westward by an high-angle fault belonging to a sinistral transtensional shear-system [28, 29, 25, 30], whereas in the eastern side it is covered by the quaternary deposits of the Biguglia plain (Fig. 1).

According to Rossi *et al*. [31], the core of the antiform is represented by the Lower Ophiolitic (LO) units, also known as Castagniccia units, characterized by successions mainly represented by calcschists with minor bodies of metabasites.

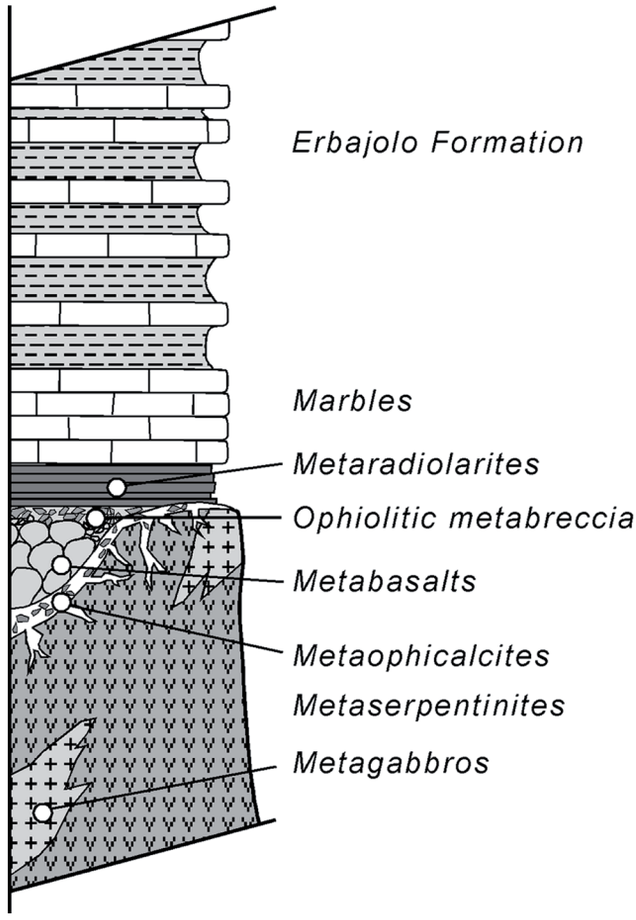

Fig. 3: Reconstructed stratigraphic column of the Lento unit.

Even if eclogite-facies metamorphism is reported by Caron and Pequignot [16], the LO units are mainly characterized by high-grade blueschist-facies overprint [17, 18].

At the top of the LO units, a complex stack of continental- and oceanic-derived (OCD) units occurs. In the study area, the OCD units includes, from bottom to the top, the Volpajola and Campitello units, folded together in a large east-verging anticline (Fig. 2). Both these units are characterized by the close association among metasediments, mainly micaschists and calcschistes with minor bodies of quarzites and marbles, metaophiolites and thin slices of ortho- and para-gneiss [32, 33, 31]. The Volpajola unit display a complex tectono-metamorphic history characterized by a metamorphic climax under eclogite-facies conditions, whereas the Campitello unit is affected by a jadeite-bearing blueschist metamorphism.

In turn, these units are overlain by the Upper Ophiolitic (UO) units represented, from bottom to the top, by the Lento and Serra Debbione units (Fig. 2). The Lento unit (partly corresponding to the Lento unit of Rossi *et al*. [31]), is characterized by a succession strongly deformed under blueschist facies metamorphism. The Lento unit is characterized by a metaophiolite sequence, probably of Middle to Late Jurassic age, consisting of a basement covered by a volcano-sedimentary complex followed by a thick metasedimentary succession (Fig.

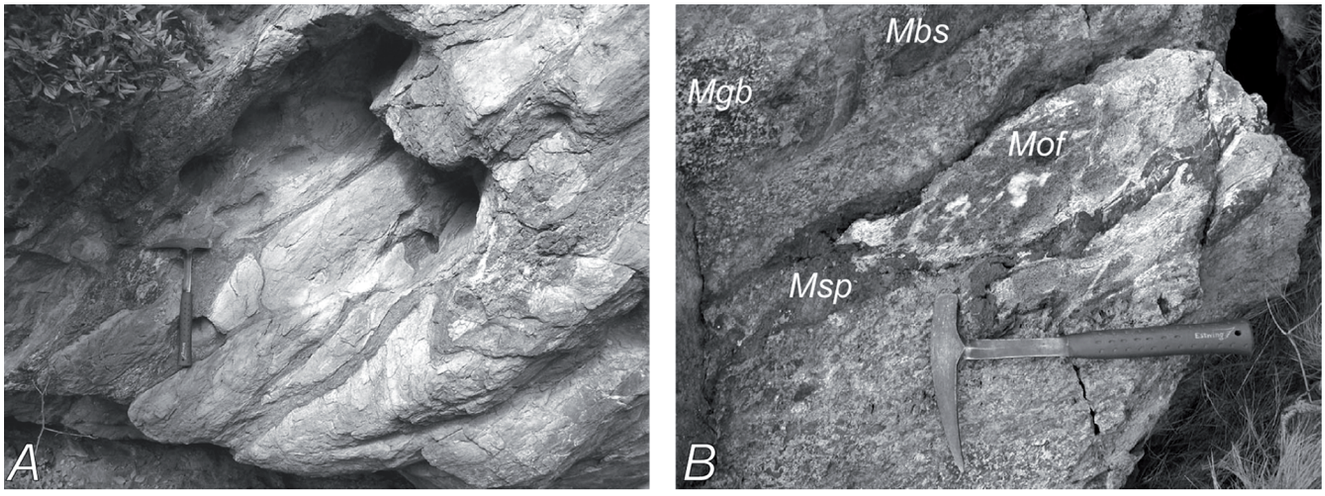

Fig. 4: A Metabasalts showing a pillow-texture; **B** Ophiolitic metabreccia: **Mgb** metagabbros; **Mbs** metabasalts; **Mof** metaophicalcites; **Msp** metaserpentinites.

3). The basement is mainly represented by metaserpentinites intruded by several gabbroic bodies and cross-cut by rare basaltic or rodingitized gabbroic dikes. In some outcrops, the metaserpentinites are topped by thin levels of metaophicalcites. The metaserpentinites are associated to metagabbros, ranging from Mg- to Fe-gabbros generally preserving their primary magmatic texture [e.g. 34]. Both metaserpentinites and gabbros are covered by a discontinuous volcano-sedimentary complex that includes both massive or pillow-lavas metabasalts and metaophiolite breccias (Fig. 4). Where the volcano-sedimentary complex is lacking, the basement shows primary relationships with the metasedimentary cover. On the whole, the ophiolite sequence of the Lento unit shows the same features of the others ophiolitic units of the Western Tethys [e.g. 35, 36 37] as, for instance, the reduced thickness, the lacking of the sheeted dike complex, and occurrence of the ophicalcites as well as the ophiolitic breccias. The metasedimentary succession includes, from the bottom to the top, a thin level of metaradiolarites, followed by a very thin and discontinuous level of marbles. The marbles are in turn topped by the Erbajolo Fm., represented by a thick succession where dm-thick micaschists and cm-thick marble layers are alternating with massive, m-thick levels of calcschistes. This succession can be compared with the Middle Jurassic to Late Cretaceous sedimentary cover of the Northern Apennine ophiolites [e.g. 38 and references].

The Lento unit is covered by the Serra Debbione unit (Fig. 2), which has been recognized for the first time during this study. This unit is characterized by a large serpentinitic body associated to minor gabbros, which in the previous studies have been referred to the Lento unit [33].

In the northwestern side of the Golo Valley, the UO units overlie the Tenda Massif, a typical large-scale dome structure represented by prevailing granitoids of Permian age and related host-rocks [25]. The relationships between the Tenda Massif and the UO units is represented by a shear zone interpreted as a low-angle detachment fault developed during the Tertiary collapse of the orogenic wedge [13, 20, 25].

4. The tectono-metamorphic history of Lento Unit

While several papers devoted to the structural history of the eclogite-facies metamorphic units from the Schistes Lustrés are available [11, 3, 4, 5, 6, 7, 8, 12, 13, 10], no reconstruction of deformation history has still now proposed for the Lento unit. Padoa [39] provided a reconstruction of the structural history of the Inzecca unit, that is generally correlated with the Lento unit by the similar lithostratigraphy and the same metamorphic grade. However, in this reconstruction the post-accretion deformations are undervaluated and their features are unrelated to the processes active in the accretionary wedges.

The proposed tectono-metamorphic history is based on original 1/10.000 geological mapping associated with meso-scale structural analysis performed throughout the whole succession of the Lento unit, from metaophiolites to metasedimentary rocks. During the geological mapping, about 30 oriented samples have been collected and studied in order to outline the main metamorphic mineral assemblages and the microstructural features. Further microscopic analyses have been performed in order to determine the relationships between the recrystallization of metamorphic minerals and their deformation structures. In addition, an estimate of metamorphic conditions is attempted by mineral chemistry analyses in order to constrain the pressure (P) and temperature (T) path during the transition from accretion to exhumation. Within the Lento unit a complex deformation history consisting of four deformation phases, hereafter referred to as D1, D2, D3 and D4, have been recognized. The later, superimposed brittle tectonics are disregarded in this paper.

4.1. Mesoscale structural features

The fabric elements of the D1 phase are poorly preserved due to the intense transposition related to the subsequent deformations, mainly those belonging to D2 phase. However, some D1 micro- and meso-structures are preserved in metabasalts, metagabbros and marble bodies, i.e. in the

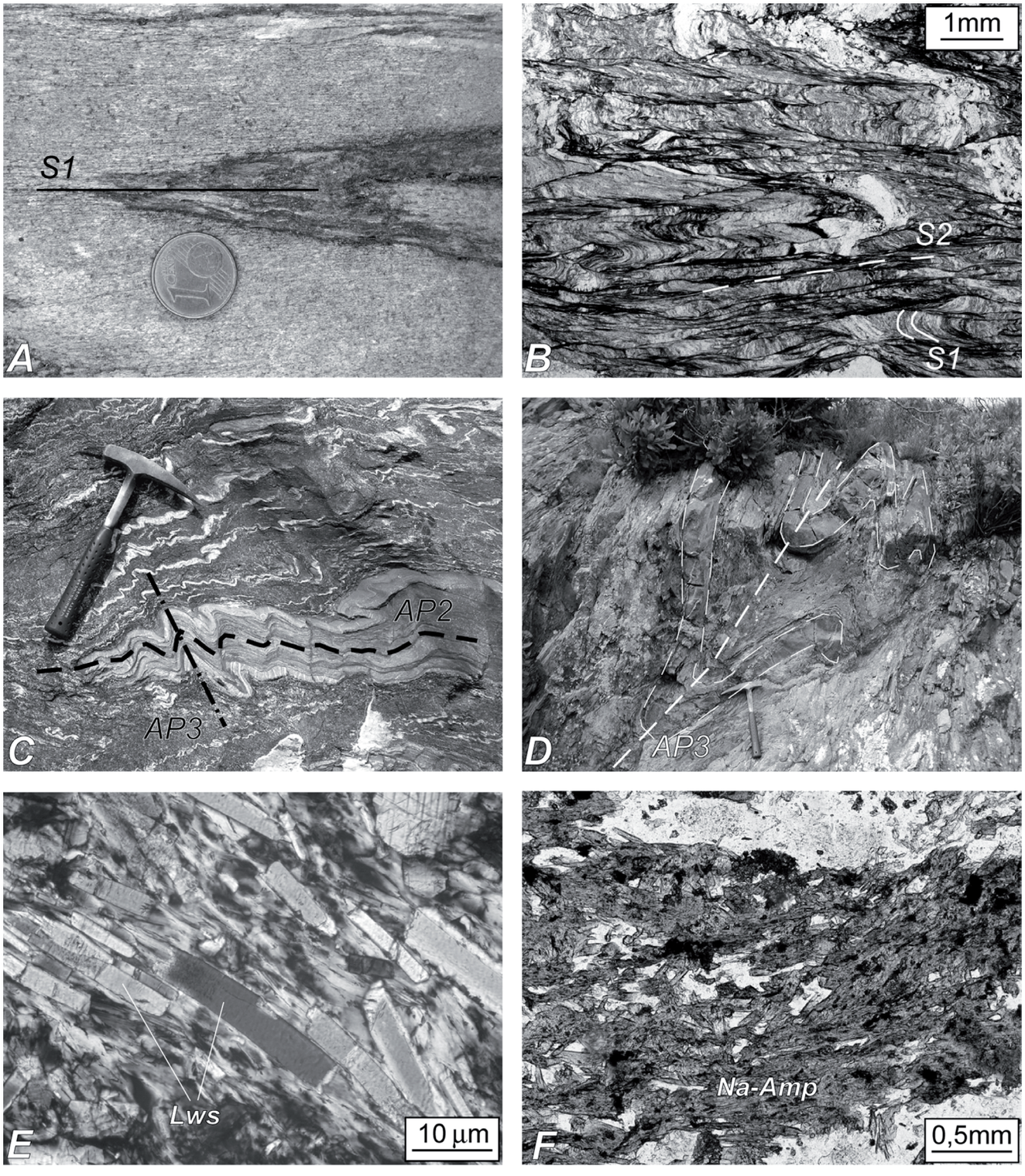

Fig. 5:. **A** Mesoascale F1 fold in the marble levels of the Erbajolo Fm.; **B** Thin section of a F2 hinge-zone developed in the Erbajolo Fm. calcschistes; **C** Mesoscale interference between F2 and F3 folds in the Erbajolo Fm.; **D** Mesoscale F3 folds in the Erbajolo Fm.; **E** Thin section (crossed polars) of metagabbros with several lawsonite crystals; **F** Thin section of metabaslts with Na-amphiboles.

low-strain domains where the D2 phase-related deformations are less transpositive. For instance, in the marble layers, the meso-scale D1 structures are represented by rare, non-cylindrical, intrafoliar isoclinal folds (Fig. 5). These folds are generally rootless with acute hinge zones and strongly thinned limbs. The A1 axes are characterized by a scattered distribution, probably related to the non-cylindrical nature of F1 folds and/or to the reorientation by later stage folding

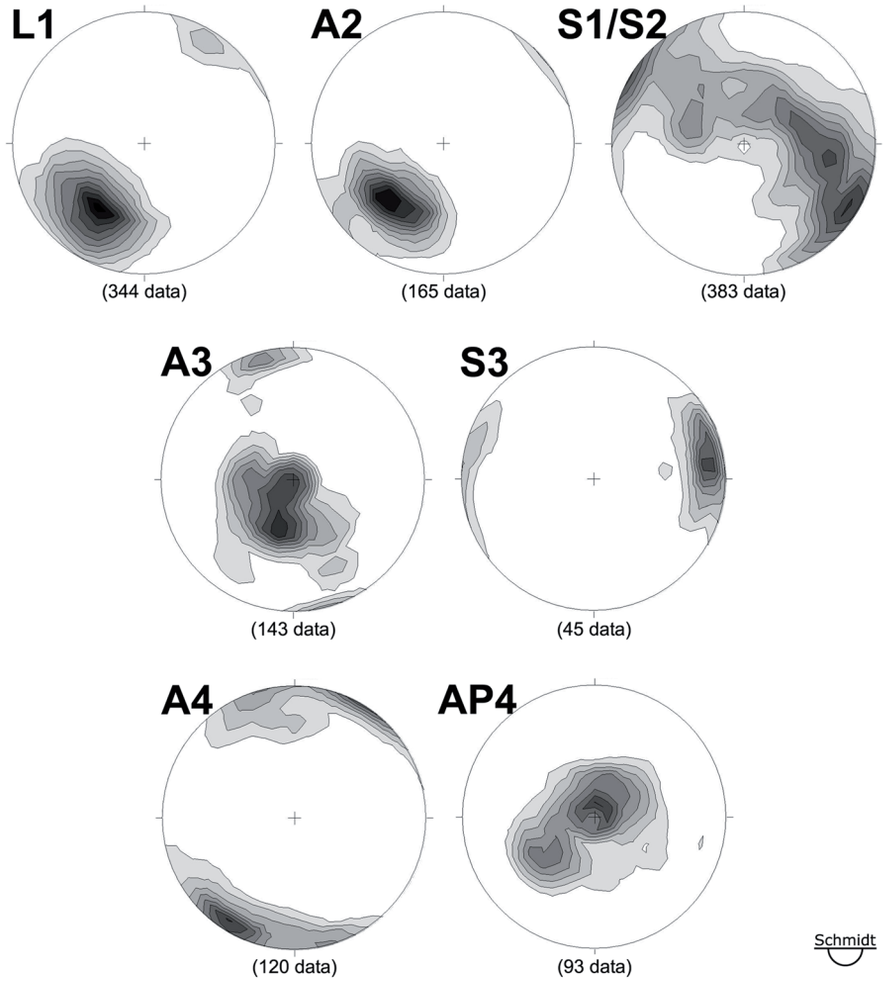

Fig. 6:. Stereographic representation (lower hemisphere, equal-area projection) of the main structural elements in the Lento Unit. **L1:** D1 phase mineral/stretching composite lineation; **A2:** F2 folds axes; **S2:** D2 phase foliation; **A3:** F3 folds axes; **S3:** D3 phase foliation ; **A4:** F4 folds axes.

phases. However, the most widespread structural elements of the D1 phase are represented by the S1 continuous foliation preserved in metagabbros and metabasalts. This S1 foliation supports a prominent L1 mineral/stretching lineation defined by prolate aggregates of quartz + calcite grains as well as preferred orientation of HP undeformed mineral grains such as Na-amphiboles, lawsonite and Cr-rich phengite. This mineral/stretching lineation shows dominant N35 trends with SW plunge (Fig. 6).

However, the most widespread deformations detected in the Lento unit can be referred to the D2 phase. At the mesoscale, the D2 phase is characterized by the F2 isoclinal folds, associated with a well developed axial-plane S2 foliation (Fig. 5). In the Erbajolo Formation, the D2 phase is represented by well developed isoclinal, cylindrical F2 folds with approximately similar geometry (class 2 and 3 of Ramsay [40]). These folds, ranging from cm to km scale, are characterized by subacute to rounded thickened hinges zones. The limbs of the F2 folds are affected by boudinage, necking and pinch-and-swell structures. The A2 axes trend strikes about N30 with moderately SW plunges (Fig. 6). The F2 folds are characterized by a well developed axial-plane foliation, generally parallel to the lithological layers (Fig. 5). In the Erbajolo Fm., mainly in the micaschists and calcschists, the S2 foliation represents the main planar anisotropy recognized in the field. This foliation, that can be classified as continuous foliation, bears shear sense indicators as σ-type tails around boudinaged quartz veins. Restored from subsequent deformations, the sense of asymmetry point out to a top-to-the northwest sense of shear. By contrast, the S2 foliation in the metabasalts, metagabbros or in the marble, when recognized, occurs as crenulation cleavage.

At the meso-scale the D3 phase is characterized by the development of F3 folds associated to a spaced S3 axial-plane foliation (Fig. 5). In the Erbajolo Fm. and in the metaradiolarites the F3 folds, showing rounded hinge zones, range from close to open with interlimb angles not exceeding 90°. They are characterized by an approximately parallel geometry (class 1B and 1C of Ramsay [40]). Large scale structures related to D3 phase have been identified in the map, mainly highlighted by the change in strike and dipping of the S2 foliation. The F3 folds always display a marked asymmetric geometry showing an eastward vergence (Fig. 2). The A3 axes strike about N-S with variable plunge angles, whereas AP3 axial planes are steeply inclined with predominately N-S strikes (Fig. 6). Generally, the mesoscale F3 folds are associated to an S3 convergent fanning axial-plane foliation, that can be classified as a crenulation cleavage in the micaschists and as disjunctive cleavage in the more competent lithotypes.

The following D4 phase is represented by structures that slightly modified the former structural setting. These structures are mainly represented by gentle to open, long wavelength (up to several meters), parallel F4 folds, although some minor scale kink-folds occur. The A4 fold axes are sub-horizontal showing a maximum clustering about N35 trend (Fig. 6), whereas the AP4 axial planes are predominately sub-horizontal. Associated to F4 folds, low-angle shear zones characterized by S-C structures are widespread. These shear zones, restored from subsequent deformation phases, display a normal fault motion with a top-to-the east sense of shear.

4.2. Microstructural features

At the micro-scale the S1 foliation can be mainly identified in thin sections from metabasalts and metagabbros. In these lithologies, the S1 foliation is everywhere preserved in the microlithons between the S2 foliation (Fig. 5). In the metabasalts, the S1 foliation can be classified as a continuous schistosity [41] defined by oriented elongate grains of Na-amphibole, phengite, quartz and albite metamorphic minerals. In the metagabbros the S1 foliation is in turn defined by Na-amphiboles, lawsonite (Fig. 5), Cr-rich phengite and minor quartz grains, the latters showing evidences of dynamic recrystallization. The S1 foliation can be rarely recognized also in the micaschists of the Erbajolo Formation, where it can be identified as relic within the microlithons along the S2 foliation, mainly in the hinge zone of the F2 folds. In this lithotype, the relic S1 foliation can be classified as a continuous cleavage, defined by a metamorphic mineral assemblage consisting of phengite, chlorite, quartz and calcite.

In thin sections of the sample collected into the limbs of the F2 folds, the S2 foliation occurs generally as continuous foliation, where the metamorphic minerals recrystallized during the D2 phase are superimposed on the pre-existing HP minerals. In these domains, the main foliation is thus represented by a composite layering defined by overprinting of S2 foliation on the S1 one. By contrast, in the F2 hinge-zone, where the S1 foliation is still preserved, the S2 foliation can be classified as crenulation cleavage, characterized by smooth cleavage domains showing a gradational to discrete transition to the microlithons [41]. In the micaschists the S2 foliation is characterized by the development of phengite, chlorite, quartz, albite, calcite. In these lithotypes, the kinematic indicators, mainly σ-type porphyroclasts of quartz and amphibole, suggest a top-to-the west sense of shear. In the metabasalts, the D2 phase-related minerals are represented by recrystallization of chlorite, quartz, albite, Ca/Na-amphibole, epidote and minor amount of sphene. The Ca/Na-amphibole typically occurs as pseudomorphs on previous Na-amphibole. In the metagabbros the S2 foliation is characterized by quartz ribbons and by the growth of chlorite and phengite around the pre-existing HP minerals. In the metaradiolarites the S2 foliation is classifiable as a disjunctive cleavage defined by white mica-rich layers separating microlithons of quartz grains. The quartz grains, characterized by a planar shape fabric, show evidences for complete dynamic recrystalization trough grain boundary migration and subgrain rotation processes (high irregular grain boundaries, gradual transition between subgrains and new grains of the same size).

At the micro-scale the S3 foliation is recognized only in the micaschists from the Erbajolo Formation. This foliation can be classified as a crenulation cleavage with smooth cleavage domains and gradational transition to the microlithons. In the micaschists, the fabric is characterized by displacement controlled strain fringes, developed around opaque minerals. The S3 foliation is characterized by the growth of quartz, calcite, chlorite and white micas.

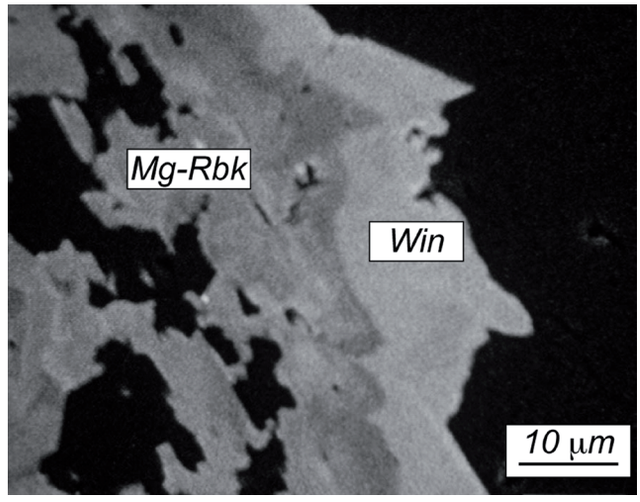

Fig. 7: SEM image showing intracrystalline variations in chemical composition, such as core-to-rim zonation, in amphiboles from sample 28/10-6. **Mg-Rbk:** Mg-riebeckite (core); **Win:** winchite (rim).

The S4 axial plane foliation corresponds to a weak and very spaced disjunctive cleavage, generally well developed in the hinge zone of the F4 folds. No metamorphic mineral assemblage related to D4 phase have been observed.

4.3. Mineral chemistry

Four samples representative of all recognized lithotypes have been selected for mineral chemistry analysis, through electron microprobe. Sample 24/4-5 is a meta-gabbro collected along the D5 Road (between Ponte Novo and Lento). This rock is characterized by a well developed composite foliation, highlighted by aligned phengite, lawsonite, chlorite and quartz ribbons, the latter showing evidences of dynamic recrystallisation. In addition, magmatic relics of pyroxene (partially or totally replaced by fine-grained Cr-rich phengite + quartz + albite aggregates) and plagioclase crystals also occur. In the meta-basalts (samples 28/10-6 and 22/4-1, see Fig. 2 for location), the S1 continuous foliation, preserved inside microlithons, is highlighted by aligned Na-amphibole, phengite, quartz and albite. In sample 28/10-6 the Na-amphiboles, showing a coarse grain-size, are characterized by core-to-rim zonation (Fig. 7). In the same samples, the S2 crenulation cleavage is defined by growth of a greenschist facies mineral assemblage (chlorite + epidote + quartz + albite + sphene). Sample 5/6-2 is a calcschist belonging to the Erbajolo Formation (outcropping along the D105 Road, Bocca di Foscatello area). It is composed of an irregular alternation of phyllosilicate-rich lepidoblastic layers and granoblastic layers made of dynamically recrystallized calcite and quartz. Inside lepidiblastic layers, the main foliation (S2) is a continuous schistosity, defined by the growth of phengite + chlorite + quartz + calcite. The S1 foliation, highlighted by aligned phengite + chlorite + quartz, is also preserved inside the microlithons.

Chemical analyses of coexisting minerals within the metamorphic assemblages were obtained using a CAMECA "SX50" electron microprobe, equipped with four wavelength-dispersive

Sample	22/4-1	22/4-1	22/4-1	22/4-1	22/4-1	22/4-1	22/4-1	28/10-6	28/10-6	28/10-6	28/10-6	28/10-6	28/10-6	28/10-6	28/10-6
Amphibole	D1-A3	D1-A6	D1-A11	D2-A2	D3-A8	D5-A8	D4-A4	Am1C	Am1R	Am2C	Am2R	Am3C	Am3R	Am4C	Am4R
Wt%															
SiO_2	57.24	57.91	58.30	58.89	57.67	58.33	57.84	53.58	54.29	53.97	54.24	56.38	54.78	55.54	54.89
TiO_2	0.05	0.05	0.03	0.09	0.06	0.08	0.03	0.21	-	0.32	-	0.61	-	-	-
Al_2O_3	11.66	10.11	7.88	10.19	6.70	8.46	8.22	4.17	1.14	4.01	1.83	4.81	1.48	2.96	1.20
Cr_2O_3	-	0.06	0.04	0.09	-	0.03	0.12	-	-	-	-	-	-	-	-
FeO tot	0.07	12.71	13.13	11.27	0.10	11.81	13.26	20.77	20.34	21.22	21.65	16.33	19.47	19.82	15.86
MnO	11.33	0.13	0.14	0.13	15.48	0.18	0.15	0.31	0.33	0.17	0.19	0.15	0.35	0.31	0.26
MgO	10.44	9.70	10.74	10.33	10.15	11.15	10.82	8.64	11.84	8.39	9.86	10.65	11.74	10.79	14.02
CaO	1.65	1.19	2.28	0.91	2.27	2.31	1.70	1.51	3.96	1.29	3.01	1.18	4.88	2.04	8.24
Na_2O	6.23	6.26	6.05	6.88	5.98	6.30	6.13	6.34	4.64	6.58	5.84	6.68	4.68	6.17	2.52
K_2O	0.01	-	0.06	0.03	0.04	0.08	0.06	-	-	-	-	-	-	-	-
Sum	98.68	98.14	98.66	98.80	98.46	98.74	98.34	95.53	96.54	95.95	96.62	96.79	97.38	97.63	96.99
Cations															
Si	7.742	7.915	7.999	7.977	7.995	7.979	7.915	7.906	7.920	7.927	7.945	7.976	7.930	7.926	7.943
Al^{IV}	0.258	0.085	0.001	0.023	0.005	0.021	0.085	0.094	0.080	0.073	0.055	0.024	0.070	0.074	0.057
SumT	8.000	8.000	8.000	8.000	8.000	8.000	8.000	8.000	8.000	8.000	8.000	8.000	8.000	8.000	8.000
Al^{VI}	1.601	1.543	1.272	1.604	1.090	1.342	1.241	0.631	0.116	0.621	0.261	0.778	0.183	0.424	0.148
Ti	0.005	0.005	0.003	0.009	0.007	0.009	0.003	0.023	0.000	0.035	0.000	0.065	0.000	0.000	0.000
Cr	0.000	0.007	0.004	0.010	0.000	0.004	0.013	0.000	0.000	0.000	0.000	0.000	0.000	0.000	0.000
Fe^{3+}	0.528	0.510	0.424	0.314	0.605	0.295	0.677	0.813	0.979	0.860	1.010	0.848	0.829	1.074	0.400
Mg	2.104	1.977	2.198	2.086	2.098	2.274	2.208	1.900	2.575	1.837	2.153	2.246	2.533	2.295	3.024
Fe^{2+}	0.753	0.942	1.083	0.962	1.190	1.056	0.839	1.632	1.330	1.647	1.576	1.063	1.455	1.206	1.428
Mn^{2+}	0.008	0.015	0.016	0.015	0.012	0.021	0.018	0.000	0.000	0.000	0.000	0.000	0.000	0.000	0.000
SumC	5.000	5.000	5.000	5.000	5.000	5.000	5.000	5.000	5.000	5.000	5.000	5.000	5.000	5.000	5.000
Mg	0.000	0.000	0.000	0.000	0.000	0.000	0.000	0.000	0.000	0.000	0.000	0.000	0.000	0.000	0.000
Fe^{2+}	0.000	0.000	0.000	0.000	0.000	0.000	0.000	0.117	0.172	0.100	0.066	0.021	0.073	0.085	0.091
Mn^{2+}	0.000	0.000	0.000	0.000	0.000	0.000	0.000	0.039	0.041	0.021	0.024	0.018	0.043	0.037	0.032
Ca	0.238	0.175	0.335	0.132	0.337	0.339	0.250	0.239	0.619	0.203	0.472	0.179	0.757	0.312	1.278
Na	1.633	1.659	1.610	1.807	1.607	1.661	1.627	1.605	1.168	1.676	1.438	1.782	1.127	1.566	0.599
SumB	1.871	1.834	1.945	1.939	1.944	2.000	1.877	2.000	2.000	2.000	2.000	2.000	2.000	2.000	2.000
Na	0.000	0.000	0.000	0.000	0.000	0.009	0.000	0.208	0.153	0.198	0.221	0.05	0.186	0.141	0.108
K	0.002	0.000	0.011	0.005	0.008	0.013	0.010	0.000	0.000	0.000	0.000	0.000	0.000	0.000	0.000
SumA	0.002	0.000	0.011	0.005	0.008	0.023	0.010	0.208	0.153	0.198	0.221	0.050	0.186	0.141	0.108

-: below detection limit

Table 1:. Representative electron microprobe analyses (wt%) of amphiboles. Structural formulae calculated assuming 23 oxygens, site assignment and ferric iron contents were calculated using the scheme proposed by Schumacher in Leake *et al.* [42] .

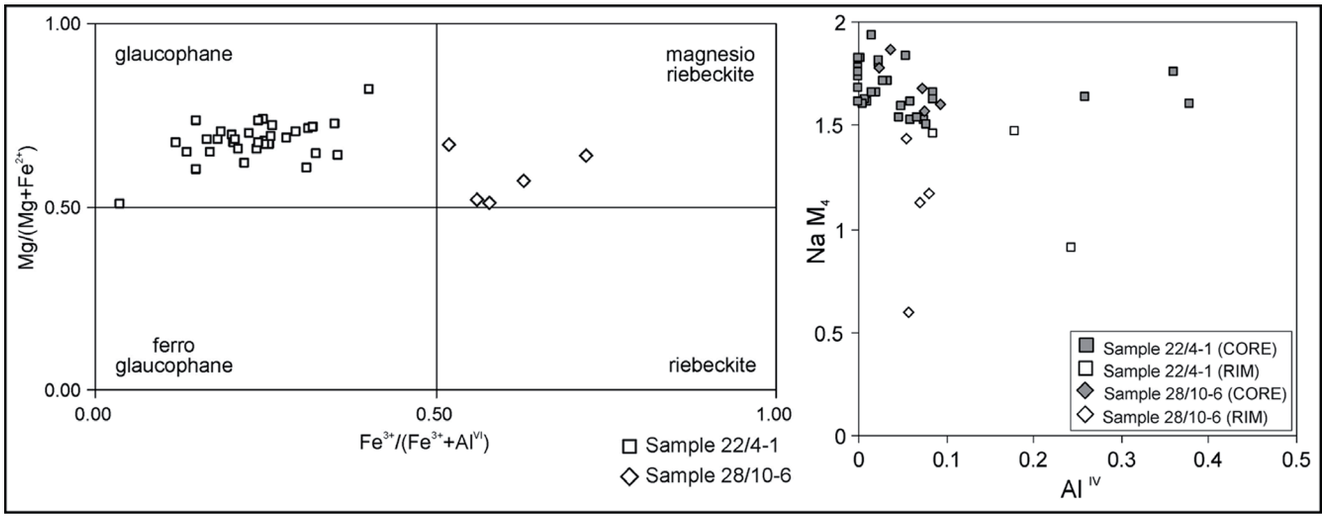

Fig. 8: Composition of sodic amphiboles: (left) classification of Leake *et al*. [42] and (right) Al^{IV} contents (apfu) *Vs*. Na in the M4 site.

spectrometers, at the *CNR - Istituto di Geoscienze e Georisorse*, *Padova*, Italy. Running conditions were 15 kV accelerating voltage and 15 nA beam current on a Faraday cage. Natural and synthetic silicates and oxides were used as standards. PAP program was employed for the correction of all data.

Amphibole. For the analyzed amphiboles, structural formulae were calculated assuming 23 oxygens, and the classification of Leake *et al*. [42] was adopted. Site assignment and ferric iron contents were calculated using the scheme proposed by Schumacher in Leake *et al*. [42]. Amphiboles from sample 28/10-6 show core-to-rim zonation. The cores are Mg-riebeckite with NaM_4 (Na in M_4 site) contents ranging from 1.57 to 1.87 atoms per formula unit (apfu) and $Mg/(Mg+Fe^{2+})$ ratios ranging from 0.51 to 0.67. The Si contents range from 7.91 to 7.98 apfu. The rims are Na/Ca-amphiboles (winchite) with NaM_4 contents ranging from 0.60 to 1.44 apfu and $Mg/(Mg+Fe^{2+})$ ratios ranging from 0.57 to 0.67. The Si contents range from 7.92 to 7.95 apfu. From core to rim, the amphiboles show a progressive decrease in Na content and an increase in Ca content (Fig. 8, Table 1). Sodic amphiboles from sample 22/4-1 are glaucophane with NaM_4 contents ranging from 1.52 to 1.93 apfu and $Mg/(Mg+Fe^{2+})$ ratios ranging from 0.60 to 0.82. They are characterized by Si contents close to the maximum of 8.00 apfu. Seldom, glaucophane crystals are characterized by a thin rim, formed by overgrowth of Na/Ca-amphibole (winchite). The winchites have NaM_4 contents ranging from 0.91 to 1.47 and $Mg/(Mg+Fe^{2+})$ ratios ranging from 0.73 to 0.55 (Fig. 8, Table 1).

Lawsonite. Lawsonite structural formulae were calculated assuming 8 oxygens and all Fe as Fe^{3+}. Analyzed lawsonites from sample 24/4-5 are very close to the ideal lawsonite composition (Table 2).

Phengite. Phengite structural formulae were calculated assuming 11 oxygens and all Fe as Fe^{2+}. If, as is likely, a small proportion of the Fe in phengite is Fe^{3+}, there would be a slight decrease in the Si content, typically <0.1 apfu, relative to the Fe^{3+}-free case [e.g. 43]. The small grain size of the phengites precluded study of intracrystalline variations in composition, so each analysis reported in Tables 3 is from a different crystal. Generally, phengites have high celadonite contents, as indicated by high Si, Mg and Fe (Table 3) relative to muscovite. The analyzed phengites from sample 24/4-5 are aligned along the S1+S2 composite foliation. They are Cr-rich phengites with a Si contents of between 3.18 and 3.43 apfu (maximum frequency of 3.40 apfu) (Table 2). Phengites analyzed from the calcschist (sample 5/6-2) are also aligned along the S1+S2 composite foliation. The Si contents, ranging from 3.12 to 3.26 apfu, are lower if compared with metabasites (Table 3).

Chlorite. Chlorite structural formulae were calculated assuming 14 oxygen and all Fe as Fe^{2+}. The small grain size of the chlorites precluded study of intracrystalline variations in composition. In samples 24/4-5, the analyzed chlorites are aligned along the S1+S2 composite foliation. They have high Si contents (between 2.85 and 2.94 apfu) and high $Mg/(Mg+Fe^{2+})$ ratios (*c*. 0.86) (Table 2). Chlorites from sample 28/10-6 have a Si contents of between 2.85 and 2.90 apfu and $Mg/(Mg+Fe^{2+})$ ratios ranging from 0.55 to 0.59. In sample 5/6-2 the analyzed chlorites are aligned along the S1+S2 composite foliation. They are characterized by variable amounts in Si and low $Mg/(Mg+Fe^{2+})$ ratios, ranging from 0.37 to 0.43 (Table 2).

4.4. Metamorphic P-T conditions in Lento unit

The different mineral assemblages developed in the lithotypes considered in this study, allow us to utilize different geothermobarometric methods to evaluate the P–T conditions of the peak metamorphism. In the meta-basalts (samples 28/10-6 and 22/4-1), the peak metamorphism is constrained by the presence, along the S1 foliation, of Na-amphibole

Sample	24/4-5	24/4-5	24/4-5	24/4-5	5/6-2	5/6-2	5/6-2	5/6-2	5/6-2	5/6-2	5/6-2	Sample	22/4-5	22/4-5	22/4-5	22/4-5
Chlorite	B2-A1	B2-A5	B4-A5	B4-A6	C1-A5	C1-A6	C1-A11	C1-A13	C2-A5	C2-A12	C3-A4	Lawsonite	B1-A1	B1-A3	B2-A3	BR-A15
Wt%												**Wt%**				
SiO_2	29.75	30.22	29.95	29.94	24.96	25.10	25.37	25.36	25.75	25.10	25.07	SiO_2	38.93	38.84	38.61	38.85
TiO_2	-	0.05	0.04	0.02	0.03	0.07	-	0.04	0.06	0.06	0.05	TiO_2	0.06	0.06	0.51	0.19
Al_2O_3	21.57	21.41	22.26	22.02	21.80	22.08	21.50	21.22	22.53	22.11	22.00	Al_2O_3	31.52	31.21	31.12	31.39
Cr_2O_3	0.06	0.05	-	0.01	0.11	0.02	-	0.01	-	0.01	0.04	Cr_2O_3	0.27	0.07	0.01	0.02
FeO tot	8.24	8.21	8.39	7.37	29.64	30.54	29.25	29.10	29.43	29.19	29.06	FeO tot	0.44	0.48	0.45	0.52
MnO	0.16	0.17	0.21	0.10	0.07	-	0.11	0.12	0.11	0.07	0.08	MnO	-	0.02	0.01	-
MgO	27.69	28.17	26.89	27.48	12.00	11.46	10.58	10.88	11.06	11.46	11.39	MgO	-	-	0.02	-
CaO	0.04	0.03	0.05	0.03	0.08	0.01	0.04	0.04	0.04	0.16	0.03	CaO	17.85	17.87	17.76	17.60
Na_2O	0.03	-	0.01	-	0.01	0.05	0.03	0.02	0.02	-	0.05	Na_2O	-	0.02	-	-
K_2O	-	0.01	-	-	0.02	-	0.19	0.09	0.24	0.04	0.04	K_2O	-	-	-	0.01
TOT	87.53	88.32	87.81	86.96	88.73	89.34	87.07	86.87	89.25	88.21	87.80	TOT	89.06	88.57	88.48	88.58
Cations												**Cations**				
Si	2.853	2.870	2.859	2.869	2.660	2.662	2.748	2.751	2.714	2.680	2.688	Si	2.028	2.034	2.024	2.032
Ti	0.000	0.004	0.003	0.001	0.003	0.006	0.000	0.003	0.005	0.005	0.004	Ti	0.002	0.002	0.020	0.007
Al	2.438	2.396	2.504	2.487	2.739	2.760	2.744	2.713	2.798	2.781	2.781	Al	1.944	1.936	1.932	1.944
Fe^{2+}	0.661	0.652	0.670	0.591	2.641	2.708	2.649	2.640	2.594	2.607	2.606	Cr	0.011	0.003	0.000	0.001
Fe^{3+}	0.000	0.000	0.000	0.000	0.000	0.000	0.000	0.000	0.000	0.000	0.000	Fe^{3+}	0.017	0.019	0.018	0.021
Mn	0.013	0.014	0.017	0.008	0.006	0.000	0.010	0.011	0.010	0.007	0.008	Mn	0.000	0.001	0.000	0.000
Mg	3.958	3.988	3.827	3.926	1.907	1.811	1.708	1.759	1.737	1.824	1.821	Mg	0.000	0.000	0.002	0.000
Ca	0.004	0.003	0.005	0.003	0.009	0.001	0.004	0.005	0.004	0.018	0.003	Ca	0.996	1.002	0.997	0.986
Na	0.006	0.000	0.002	0.000	0.003	0.011	0.007	0.004	0.005	0.000	0.011	Na	0.000	0.000	0.000	0.001
K	0.000	0.002	0.000	0.000	0.002	0.000	0.026	0.012	0.033	0.006	0.005	K	0.000	0.000	0.000	0.001
Sum	9.931	9.929	9.887	9.886	9.970	9.958	9.896	9.898	9.901	9.928	9.926	Sum	4.998	4.999	4.995	4.993

-: below detection limit

Table 2: Representative electron microprobe analyses (wt%) of chlorites (structural formulae calculated assuming 14 oxygen and all Fe as Fe^{2+}) and lawsonites (structural formulae calculated assuming 8 oxygens and all Fe as Fe^{3+}).

Sample	5/6-2	5/6-2	5/6-2	5/6-2	5/6-2	5/6-2	5/6-2	5/6-2	5/6-2	5/6-2	24/4-5	24/4-5	24/4-5	24/4-5	24/4-5
Phengite	C1-A1	C1-A9	C1-A15	C2-A4	C2-A7	C2-A8	C2-A10	C3-A3	CR-A6	CR-A9	B3-A1	B3-A5	B5-A5	B5-A6	B4-A4
Wt%															
SiO_2	48.49	49.09	49.29	49.27	48.77	49.52	48.85	46.16	48.93	48.55	51.27	51.77	51.50	51.42	50.86
TiO_2	0.12	0.13	0.01	0.12	0.10	0.15	0.05	2.04	0.11	0.23	0.09	0.05	0.05	0.09	0.04
Al_2O_3	32.64	32.01	33.71	32.15	32.29	32.97	32.21	30.80	32.95	33.68	28.14	28.37	21.79	27.15	29.01
Cr_2O_3	0.07	0.05	0.06	0.07	0.02	-	0.05	0.01	0.02	0.01	0.09	-	8.01	1.15	0.03
FeO tot	1.41	1.85	1.16	1.94	1.50	1.47	1.70	4.00	1.48	2.70	0.57	0.68	0.77	0.59	0.46
MnO	-	0.04	-	-	0.02	0.03	-	0.04	0.03	-	0.01	-	-	0.03	0.02
MgO	1.62	1.80	1.43	1.73	1.65	1.44	1.68	2.26	1.61	1.55	4.68	3.81	4.37	3.82	3.54
CaO	0.02	0.09	0.01	0.02	0.03	0.06	0.03	0.12	0.04	0.12	0.02	0.01	0.02	0.01	-
Na_2O	0.86	0.47	0.70	0.60	0.70	0.50	0.98	0.82	0.60	0.73	0.34	0.33	0.16	0.25	0.26
K_2O	9.32	9.50	9.31	9.24	9.58	10.01	9.39	7.99	9.37	8.98	10.12	10.23	10.28	10.11	10.47
TOT	94.56	95.02	95.68	95.12	94.68	96.15	94.94	94.25	95.14	96.55	95.33	95.24	96.94	94.61	94.69
Cations															
Si	3.226	3.255	3.228	3.259	3.244	3.245	3.244	3.123	3.232	3.177	3.381	3.413	3.434	3.423	3.377
Al^{IV}	0.774	0.745	0.772	0.741	0.756	0.755	0.756	0.877	0.768	0.823	0.619	0.587	0.566	0.577	0.623
Sum Z	4.000	4.000	4.000	4.000	4.000	4.000	4.000	4.000	4.000	4.000	4.000	4.000	4.000	4.000	4.000
Al^{VI}	1.785	1.757	1.829	1.764	1.776	1.791	1.764	1.578	1.796	1.773	1.568	1.617	1.146	1.553	1.646
Ti	0.006	0.006	0.001	0.006	0.005	0.007	0.002	0.104	0.006	0.011	0.005	0.002	0.002	0.005	0.002
Cr	0.004	0.003	0.003	0.004	0.001	0.000	0.003	0.001	0.001	0.001	0.005	0.000	0.422	0.060	0.002
Fe^{3+}	0.000	0.000	0.000	0.000	0.000	0.000	0.000	0.000	0.000	0.000	0.000	0.000	0.000	0.000	0.000
Fe^{2+}	0.078	0.102	0.063	0.107	0.083	0.080	0.094	0.226	0.082	0.148	0.031	0.037	0.043	0.033	0.025
Mn	0.000	0.002	0.000	0.000	0.001	0.002	0.000	0.002	0.002	0.000	0.001	0.000	0.000	0.002	0.001
Mg	0.160	0.177	0.139	0.171	0.164	0.141	0.166	0.228	0.159	0.151	0.460	0.374	0.434	0.379	0.350
Sum Y	2.034	2.048	2.035	2.051	2.031	2.021	2.030	2.139	2.045	2.084	2.069	2.031	2.048	2.031	2.026
Ca	0.002	0.006	0.001	0.001	0.002	0.004	0.002	0.009	0.003	0.008	0.001	0.001	0.002	0.001	0.000
Na	0.111	0.060	0.089	0.077	0.090	0.064	0.126	0.108	0.077	0.092	0.044	0.042	0.021	0.032	0.033
K	0.791	0.803	0.778	0.779	0.812	0.836	0.795	0.689	0.789	0.749	0.851	0.860	0.874	0.859	0.886
Sum X	0.903	0.870	0.867	0.858	0.905	0.904	0.923	0.805	0.869	0.850	0.896	0.903	0.896	0.891	0.919
TOT	6.937	6.918	6.902	6.909	6.936	6.925	6.953	6.944	6.913	6.934	6.966	6.933	6.944	6.922	6.946

-: below detection limit

Table 3: Representative electron microprobe analyses (wt%) of phengites. Structural formulae calculated assuming 11 oxygens and all Fe as Fe^{2+}.

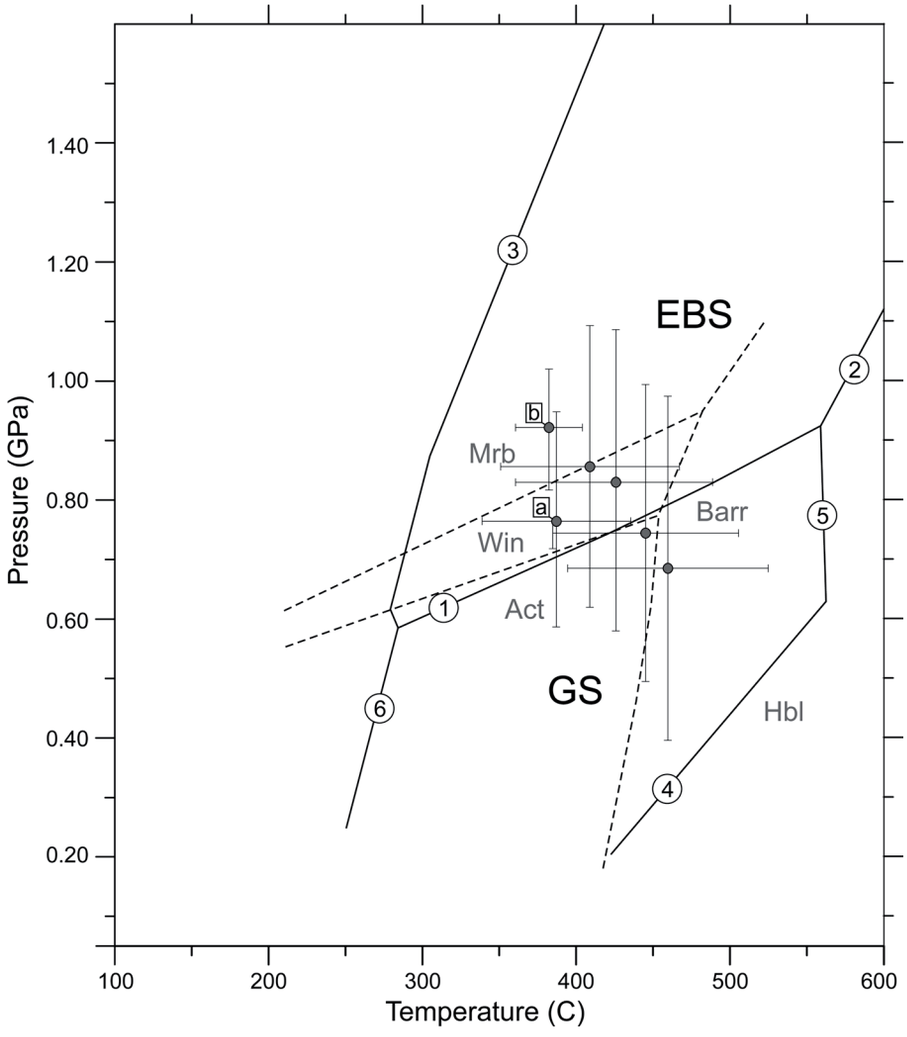

Fig. 9: Estimated peak metamorphic pressure-temperature (P-T) conditions. P–T grid for epidote–blueschist facies (continuous lines) following Na-amphibole composition no. 5 of Evans [46] , abbreviations: EBS epidote–blueschist facies; GS geenschist facies; **1** Gln + Czo + Qtz + W = Ab + Chl + Tr; **2** Gln + Czo + Qtz = Ab + Prp + Tr + W; **3** Czo + Gln + Qtz + W = Lws + Di + Jd; **4** Chl + Czo + Qtz = An + Tr + W; **5** Chl + Czo + Qtz = Prp + Tr + W; **6** Pmp + Chl + Qtz = Czo + Tr + W; **Ab:** albite; **An:** anorthite; **Cel:** celadonite; **Chl:** chlorite; **Czo:** clinozoisite; **Di:** diopside; **Gln:** glaucophane; **Jd:** jadeite; **Lws:** lawsonite; **Phl:** phlogopite; **Pmp:** pumpellyite; **Prp:** pyrope; **Qtz:** quartz; **Tr:** tremolite; **W:** water. Winchite stability field (dashed lines) of Banno and Sakai [45] and Otsuki and Banno [47] based on the hematite-bearing schists of Sanbagawa Belt (Japan), abbreviations: **Mrb:** Mg-riebeckite: **Win:** winchite; **Act:** actinolite; **Barr:** barroisite; **Hbl:** hornblende. The points represent the average pressure and temperature (P-T) estimates and their associated standard deviations (σP and σT) calculated for each chlorite-phengite pair (sample 5/6-2) using local equilibria method [55] . **a** average P-T for assemblage shown in the diagram from Figure 10a; **b** average P-T for assemblage shown in the diagram from Figure 10b.

(core of analyzed amphiboles), coexisting with phengite, quartz and albite. The Na-amphibole is a typical mineral related to the blueschist facies and is indicative of HP/LT gradient metamorphism [e.g. 44, 45, 46, 47]. The minimum pressure (P) conditions of this mineral assemblage, can be estimated using the P–T grid for the epidote-blueschist facies of Evans [46], calculated in the NCMASH (Na_2O + CaO + MgO + Al_2O_3 + SiO_2 + H_2O) system assuming a_{H2O}=0.9. Figure 9 reports the P–T grid calculated for Na-amphibole composition no. 5 [46], which is similar to that of Mg-riebeckite/glaucophane from the studied rocks. Since no Ca-Al silicate phase (e.g. epidote, pumpellyte, lawsonite) is present in these samples, temperature is difficult to estimate. This absence may be due to the inappropriate protolith chemistry, and/or high CO_2 content in fluid during metamorphism [e.g. 48]. According to the semi-quantitative phase diagram of amphiboles proposed by Banno and Sakai [45] and Otsuki and Banno [47], as no hornblende or barroisite are present in the studied metamorphic assemblages, temperatures are estimated to have been below 450°C. For temperatures lower than 450 °C, the minimum pressure estimated from the P–T grid for the epidote-blueschist facies [46] is about 0.60-0.80 GPa (Fig. 9).

The analyzed amphiboles show intracrystalline variations in chemical composition, such as core-to-rim zonation, as testified by the epitaxial overgrowths of Na/Ca-amphibole (winchite). Therefore the amphiboles show a progressive decrease in NaM_4 (Na content in the M4 site) and an increase in Ca content from core to rim. According to the phase diagram shown by Banno and Sakai [45] and Otsuki and Banno [47], the estimated stability field for winchite overlaps with the blueschist / greenschist transition, therefore winchite rims around Mg-riebeckite and glaucophane cores testify a retrograde relationship (Fig. 9). In the studied meta-basalts, retrograde metamorphic conditions are also testified by the presence of greenschist facies mineral assemblages (chlorite + epidote + quartz + albite + sphene), growth parallel to the S2 foliation.

In the other samples (24/4-5 and 5/6-2), the peak metamorphism is characterized by the mineral assemblage phengite + chlorite + quartz ± albite ± lawsonite ± calcite. Phengite and chlorite are widespread minerals in rocks metamorphosed over a wide range of pressure and temperature (P-T) conditions, and their compositions depend on the P-T conditions prevailing during their formation; particularly Si content of phengites depends on pressure and Al^{IV} content of chlorites depend on temperature [e.g. 49, 50, 51, 52, 53, 54]. For these reasons,

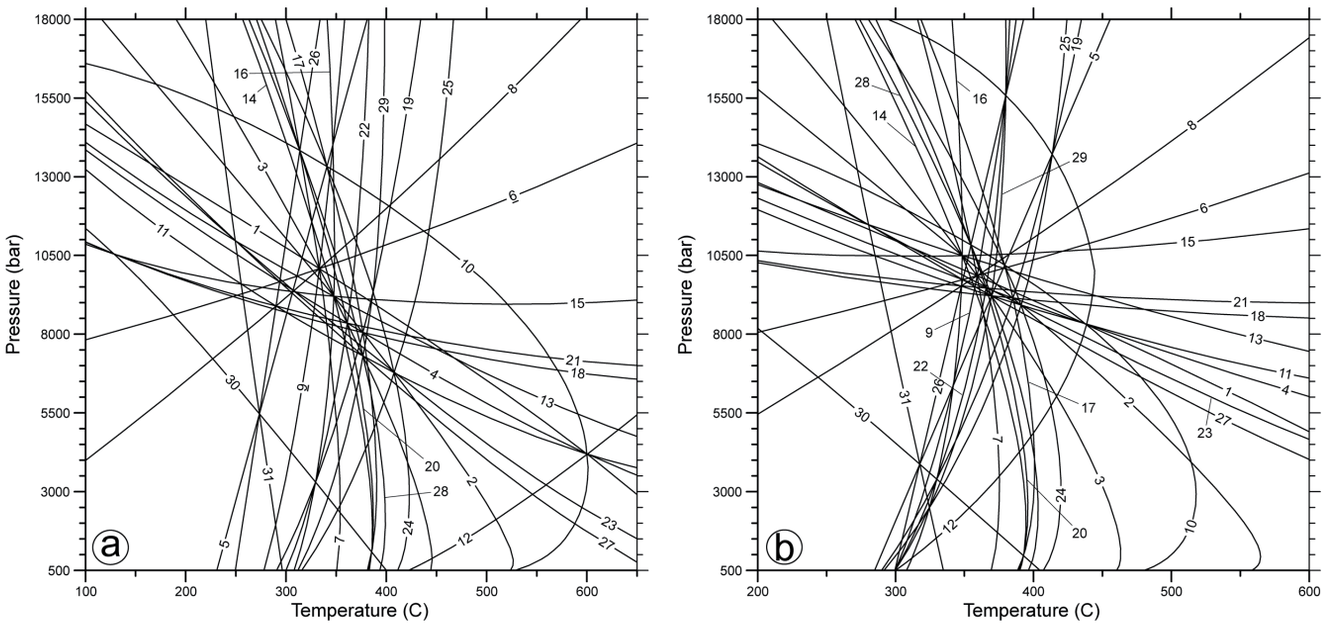

Fig. 10: Examples of P-T plot of chlorite + phengite + quartz + H_2O equilibrium in sample 5/6-2 (Erbajolo Fm.). Reaction curves **1:** 8 Prl + 10 Mg-ACel + 2 Daph + 4 W = 5 Sud + 10 Fe-ACel + 23 Qtz; **2:** 8 Prl + 2 Clin + 4 W = 5 Sud + 23 Qtz; **3:** 2 Prl + Ames + 2 W = 2 Sud + 4 Qtz; **4:** 2 Mg-ACel + 4 Prl = 15 Qtz + 2 Ms + Sud; **5:** Daph + 5 Mg-ACel = 5 Fe-ACel + Clin; **6:** 2 Daph + 10 Mg-ACel + 4 Prl = 15 Qtz + 10 Fe-ACel + 2 Ames + Sud; **7:** 14 Prl + 40 Fe-ACel + 23 Ames + 30 W = 26 Sud + 8 Daph + 40 Mg-ACel; **8:** 4 Daph + 20 Mg-ACel + 6 Prl = 26 Qtz + 20 Fe-ACel + 5 Ames + 2 W; **9:** 3 Sud + 2 Daph + 10 Mg-ACel = 7 Qtz + 10 Fe-ACel + 4 Ames + 4 W; **10:** 14 Prl + 23 Ms + 52 Mg-ACel + 15 Daph + 30 W = 26 Sud + 75 Fe-ACel; **11:** 5 Fe-ACel + 6 Prl = 26 Qtz + 5 Ms + Daph + 2 W; **12:** 3 Sud + 10 Fe-ACel = 7 Qtz + 4 Ms + 6 Mg-ACel + 2 Daph + 4 W; **13:** 2 Clin + 4 Prl = 15 Qtz + 2 Ames + Sud; **14:** 14 Prl + 23 Ames + 30 W = 26 Sud + 8 Clin; **15:** 4 Clin + 6 Prl = 26 Qtz + 5 Ames + 2 W; **16:** 3 Sud + 2 Clin = 7 Qtz + 4 Ames + 4 W; **17:** 14 Prl + 23 Ms + 15 Clin + 30 W = 26 Sud + 23 Mg-ACel; **18:** 5 Mg-ACel + 6 Prl = 26 Qtz + 5 Ms + Clin + 2 W; **19:** 3 Sud + 4 Mg-ACel = 7 Qtz + 4 Ms + 2 Clin + 4 W; **20:** 14 Prl + 8 Ms + 15 Ames + 30 W = 26 Sud + 8 Mg-ACel; **21:** 4 Mg-ACel + 6 Prl = 26 Qtz + 4 Ms + Ames + 2 W; **22:** 3 Sud + 2 Mg-ACel = 7 Qtz + 2 Ms + 2 Ames + 4 W; **23:** 2 Clin + 10 Fe-ACel + 20 Prl = 75 Qtz + 10 Ms + 2 Daph + 5 Sud; **24:** 70 Prl + 115 Ms + 52 Clin + 23 Daph + 150 W = 130 Sud + 115 Fe-ACel; **25:** 15 Sud + 20 Fe-ACel = 35 Qtz + 20 Ms + 6 Clin + 4 Daph + 20 W; **26:** Daph + 4 Mg-ACel + Ms = 5 Fe-ACel + Ames; **27:** Ames + 5 Fe-ACel + 8 Prl = 30 Qtz + 5 Ms + Daph + 2 Sud; **28:** 14 Prl + 10 Ms + 13 Ames + 2 Daph + 30 W = 26 Sud + 10 Fe-ACel; **29:** 6 Sud + 5 Fe-ACel = 14 Qtz + 5 Ms + 3 Ames + Daph + 8 W; **30:** Mg-ACel + Ames = Clin + Ms; **31:** 5 Fe-ACel + 5 Ames = Daph + 4 Clin + 5 Ms. Key **Sud**: $(sudoite)_{Chl}$; **Daph:** $(daphnite)_{Chl}$; **Clin:** $(clinochlore)_{Chl}$; **Ames:** $(amesite)_{Chl}$; **Fe-ACel:** $(Fe\text{-}Al\text{-}celadonite)_{Phe}$; **Mg-ACel:** $(Mg\text{-}Al\text{-}celadonite)_{Phe}$; **Ms:** $(muscovite)_{Phe}$; **Prl:** $(pyrophyllite)_{Phe}$; **Qtz:** quartz; **W:** water.

chlorite and phengite are good candidates for thermobarometric estimates. The technique of chlorite-phengite multi-equilibrium calculation based on the assumption of local equilibrium has been used in the present study to constrain the P-T conditions of metamorphism for the samples in which typical minerals index of blueschist facies are not preserved. In sample 5/6-2 (calcschist belonging to the Erbajolo Formation), several pairs of chlorite-phengite, mainly arranged parallel to the S1 foliation, were analyzed. The chlorite-phengite pairs used to perform the thermodynamic calculation were first selected using classical criteria suggesting equilibrium: the selected pairs involve mineral in contact, which do not present evidences of reaction and growth in the same microstructures (e.g. schistosity, strain shadow, shear band, etc…). According to Vidal and Parra [55], a further selection of the analyses was made on the basis of the chemical criteria aimed at rejecting mineral compositions that are not a linear combination of the end-members used in the chlorite and white mica solid-solution models. The solid solution model for white mica is from Parra *et al*. [56]. On the base of compositional variations of analyzed white micas, the following end-members: Mg-Al-celadonite (Mg-ACel), Fe-Al-celadonite (Fe-ACel), pyrophyllite (Prl) and muscovite (Ms) were used for calculation. The solid solution model for chlorite is from Vidal *et al*. [54] and the end-members used for the P-T estimate were: amesite (Ames), sudoite (Sud), clinochlore (Clin) and daphnite (Daph). In the system K_2O - Al_2O_3 – FeO – MgO - SiO_2 - H_2O, with these four white mica and four chlorite end-members, the equilibrium P-T conditions for the chlorite + phengite + quartz + H_2O equilibrium in sample 5/6-2 are given by the intersection of 31 equilibria, 4 of which are independent (Fig. 10). The thermodynamic calculation used in the present study were performed with TWEEQ software [57]. The thermodynamic data and the solid solution models are from Berman [58, 59] for all phases except K-white mica and chlorite, for which the models of Parra *et al*. [56] and Vidal *et al*. [54] were used,

respectively. The average pressure and temperature (P-T) estimates and their associated standard deviations (σP and σT) were calculated for each mineral pair with the INTERSX software included in the TWQ 2.01 package [57].

Calculated Chl + Phe + Qtz + H_2O equilibrium P-T conditions using different chlorite-phengite pairs from the same thin section (5/6-2) are shown in Figure 9. The P-T points constrained by the composition of associated chlorite and phengite define a field in the diagram, corresponding to the low-grade blueschist facies metamorphic conditions (P=0.80±0.20 GPa, T=400±50 °C).

Even if the P-T estimation from sample 5/6-2 is determined by few points, the peak metamorphic P-T conditions are consistent with the data provided by the metamorphic mineral assemblages including Na-amphibole.

Summing up the available thermobarometric information, the peak metamorphic conditions acquired during the D1 deformation phase can be estimated as P= 0.80±0.20 GPa and T<450 °C (epidote-blueschist facies), while the D2 phase is associated to retrograde metamorphic assemblages, characterized by P-T conditions consistent with the blueschist/greenschist facies transition. Finally the D3 phase is characterized by the growth of very low-grade mineral assemblages, such as, quartz + calcite + chlorite + white mica.

5. Discussion

The structural features of the Lento unit can be compared to that of the other ophiolitic units from the Western Alps and Northern Apennines, whose deformations have been interpreted as achieved within an accretionary wedge of a subduction zone, as proposed since long time [e.g. 60, 61, 62 and many others]. According to its structural features, the evolution of the Lento unit can be subdivided into accretion- and exhumation-related stages.

5.1. Accretion-related stage

The D1 phase and the associated HP metamorphism recognized in the Lento unit can be regarded as achieved during its accretion in a Late Cretaceous subduction zone (Fig. 11), according to available radiometric dating [15, 19]. As recognized also in similar units of Western Alps and Northern Apennines, the material accreted to the wedge includes both the ophiolites and the sedimentary covers. The accretion of the ophiolites is probably connected with the peculiar stratigraphy of the oceanic lithosphere of the Ligure-Piemontese, characterized by multiple levels inherited from the oceanic history and able to drive the detachment of large slices of basic rocks. The Lento unit show a well preserved stratigraphy without development of mèlange-type rocks, indicative of an accretion process by a coherent underplating [63, 64, 65, 66, 67]. The depth of the accretion is provided by T and P conditions of the metamorphic climax, indicative of a deformation at 25-30 km. The structural features of the D1 phase, consisting of rootless isoclinal folds, bedding-parallel foliation, mineral-stretching lineations and HP metamorphism, are coherent with deformation achieved in the subduction channel during the accretion process [63, 64, 68, 69, 70, 71]. In this tectonic setting, as result of the high strain values of non-coaxial deformation, the

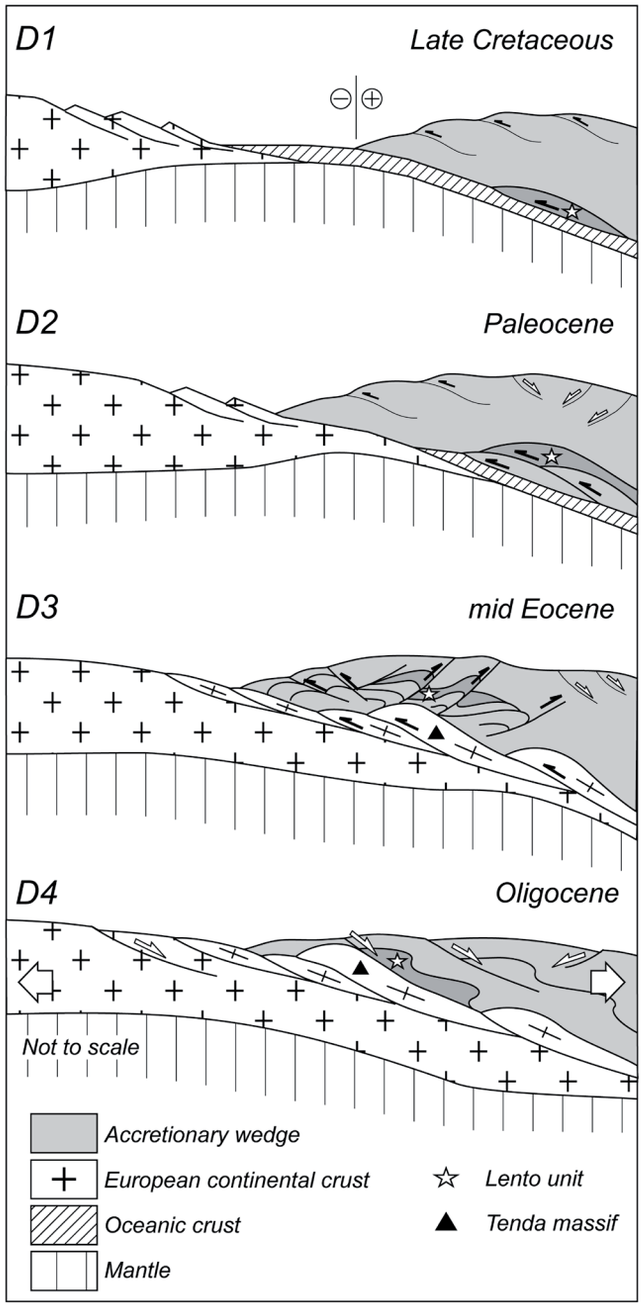

Fig. 11: Geodynamic model of the Lento unit tectono-metamorphic history. **D1** coherent underplating of the Lento unit at a depth of about 25-30 km; **D2** transition from accretion to exhumation, achieved by the development in the accretionary wedge of a duplex structure at depth and coeval syntectonic erosion and normal faulting in its upper part; **D3** second stage of exhumation, achieved during a further horizontal shortening with development of east-verging backthrusts and backfolds structures; **D4** extensional event representing the final exhumation of the Lento unit.

mineral-stretching lineations are assumed to be aligned along the shear direction [71 and quoted references]. In the Schistes Lustrés complex of the Alpine Corsica, high pressure-related mineral-stretching lineations show a scattered trends. In the northern sectors (Cap Corse area) these lineations show E-W trend, orthogonal to the belt direction [72, 6, 7], although in different zones (Punta di Canelle) N-S lineations have been recognized [6, 7]. In the southern sectors (Castagniccia area) these lineations show quite scattered trends, even if a N-S trend seems to be prevailing [73, 20]. This differences in strike of the L1 lineations recognized along the Schistes Lustrès complex has been generally interpreted as the result of the subsequent deformations, able to produce a sharp reorientation of the preexisting structures [e.g. 73]. However, in the Golo Valley area, where both the A2 and A3 axes display a N30 strike, the L1 direction, that are mainly oriented about N30, can be regarded as little re-oriented by the subsequent structures. So, the recognized L1 trend of Lento unit reflects the pristine trend of the displacement during the D1 phase. According to structural studies from both orogenic belts and numerical models [e.g. 74], the oblique subduction produces within the accretionary wedge a deformation partitioned in two displacement components, respectively orthogonal and parallel to the trench axis, which contemporaneously operate in different structural domains. In addition, the analogue models [75] also suggest that above a value of convergence obliquity, a large and well distinct wrenching-dominated zone is developed at the rear of the imbricate thrusts wedge located in front of the accretionary wedge. The D1 deformation phase can be hypothesized as acquired by the Lento unit in this wrenching-dominated domain. This conclusion fit very well with the reconstruction proposed by Harris [6, 7] that interpreted the recognized change in the HP stretching lineation trend as the result of an oblique subduction, producing through time an alternance of trench-parallel and trench-orthogonal displacements.

5.2. Exhumation-related stage

The post-D1 phase deformations can be related to the exhumation history developed before the Miocene, i.e. the age of sedimentary deposits that seal all the deformations observed in the units of Schistes Lustrés Complex. The pre-Miocene age of these deformation is also confirmed by radiometric dating available for the Schistes Lustrés Complex, that indicate a progressive exhumation older than 25 ma [19].

Microstructural observations and mineral chemistry data presented in this study show that the transition from the D1 to the D2 phase was characterized by the continuous development of reaction rims around the metamorphic amphiboles. Moreover, the metamorphic mineral assemblages associated to the S1 and S2 foliations is here interpreted as recording a decompressional but near isothermal transition from blueschist to greenschist facies conditions. However, although this pressure decrease suggests the onset of an exhumation processes, the structural features of the D2 phase do not show any evidence of extensional deformations, generally regarded as the responsible of this type of geodynamic process. By contrast, the D2 phase is characterized by NW-verging isoclinal folds with strongly thinned or boudinated limbs and by a pervasive foliation parallel to the stratigraphic bedding, both indicative of a prevailing deformation similar to that recognized for the D1 phase. Taking into account both structural and metamorphic evidences, the D2 phase seems to be developed during the first stages of exhumation by a further shortening event (Fig. 11). Analogue-numerical modeling approach [76 and quoted references] shows that the exhumation in the accretionary wedges depends by combined tectonic and erosional processes. In an accretionary wedge affected by complementary processes as syntectonic erosion and normal faulting in its upper part, the development of a duplex structure at depth may result in the exhumation of the previously accreted material. As observed in present-day and fossil examples [63, 64, 66] and by analogue modeling techniques [77, 78], the duplex structure consists by a series of thrusts, whose dipping and location mainly depend by the basal friction at the base of the accretionary wedge [76]. The deformations postulated for this type of process [63, 64, 66] seems to be coherent with those observed in the Lento unit during the D2 phase. So, this phase can be tentatively interpreted as the result of a post-accretion development of a duplex structure at the depth of the accretionary wedge. The development of this structure is here hyphotized to produce exhumation by interactions between translation upward of the Lento unit, pushing at the rear by the newly accreted units, and removal of material in upper part of the accretionary wedge by erosion and normal faulting.

The following D3 phase can be connected with a further shortening event characterized by asymmetric E-verging folds associated to steeply dipping S3 axial plane foliation. This foliation is characterized by low-grade metamorphic assemblages that indicates a shallower deformation level with respect to that of the D2 phase. The F3 folds are also recognized in the other units of the Golo Valley, suggesting that the D3 phase is a widespread event in the Schistes Lustrés complex. However, the main difference between D2 and D3 phase consists in a sharp change of the shear sense, top-to-the northwest for the D2 phase vs. top-to-the east for the D3 phase. This change probably occurred as result of a main geodynamic event, able to produce a sharp shortening of the accretionary wedge with development of both lower and upper plate verging deformations. This type of deformations can be envisaged as result of the processes related to the continental collision (Fig. 11). This interpretation fit very well with the reconstruction proposed by Malavieille *et al*. [10], where the Late Cretaceous-Paleocene accretionary wedge experienced sharp shortening during the Middle to Late Eocene extrusion of the previously subducted continental crust.

The Lento unit deformation history ends with the D4 phase, characterized by flat-lying axial-planes and horizontal fold axes indicating a prevailing eastward facing. This deformation can be interpreted as originated from vertical shortening and

folding of preexisting nonhorizontal layers, during a ductile extensional tectonics, such as recognized in other areas of the Alpine belt (Fig. 11) [79, 80, 81]. Differently from the eclogite-facies oceanic units, no metamorphic mineral assemblage related to D4 phase have been observed. This occurrence can be probably explained by the more shallow depth reached by the Lento unit before the inception of extensional tectonics. As described by Fournier *et al*. [12], Jolivet *et al*. [13, 18], Daniel *et al*. [20] and Brunet *et al*. [19], the D4 deformations was probably acquired during the Oligocene-Miocene extensional tectonics related to collapse of the orogenic wedge.

6. Conclusions

According to previous discussed reconstruction of the deformation history, some conclusions can be drawn about the tectonic history of the Lento unit.

The Lento unit can be regarded as a coherent unit deeply deformed during the D1 phase under HP metamorphic conditions. According these features, the D1 phase can be regarded as related to an accretion event in a subduction zone, by coherent underplating at a depth of about 25-30 km. This interpretation of the D1 phase recognized in the Lento unit, as well as in the other oceanic unit of Corsica, as for instance the Balagne Nappe [e.g. 27], is in broad agreement with the evidence for the occurrence in the Late Cretaceous of an Alpine accretionary wedge ("protoCorsican belt" of Malavieille *et al*. [10]), developed before the continental collision. This belt was consisting of oceanic units with different peak metamorphic conditions, from prehnite-pumpellyte to blueschists and eclogite facies, depending by respective depth of accretion. However, the most interesting data collected in the Lento unit is represented by the orientation of the L1 mineral-stretching lineations, that are characterized by a N35 strike. This orientation seems to be an original feature, that is contrasting with the data from the other areas of the Schistes Lustrés complex, where a E-W trend is reported. The available data are still scarce and more information are required, but these features are coherent with an oblique convergence, as proposed by Harris [6, 7] in the Alpine Corsica and by Marroni and Treves [82] in the Northern Apennine.

The subsequent deformation phases can be referred to the exhumation history, as suggested by the continuous decrease of metamorphic conditions from D1 to D4 phase.

The transition from accretion to exhumation is represented by the D2 phase, whose structural elements are the most widespread at both micro- and meso-scale. According to its features, the D2 phase can be regarded as a first stage of the exhumation in an accretionary wedge affected by syntectonic erosion. This exhumation is achieved by the accreted units during the development of a duplex structure resulting from the continuous underplating at deep [e.g. 81]. This type of deformation has been also described for the paleoaccretionary wedge system from Okinawa Island, Japan [83] and Cretan Island in Greece [84].

The D3 phase represents a further step in the exhumation of Lento unit. According to the structural features, also this deformation seems to be acquired by a further horizontal shortening, even if characterized by top-to-the east shear sense, opposite to the top-to-the northwest shear sense detected for the D2 phase. This change can be tentatively correlated to the inception of the continental collision, that produced a strong shortening of the preexisting accretionary wedge with development of a both east- and west- verging deformations.

The D4 phase, characterized by flat-lying axial-planes and horizontal fold axes indicating a vertical shortening, represents the final stage of the exhumation of the Lento unit. The features of this phase was acquired during an extensional event, the represent the final stage of the exhumation of the Lento unit.

Finally, the data collected for the Lento unit suggest that the resulting picture for the exhumation is more complex that previous described [e.g. 12, 13, 20] and includes three events with different features. The first two phases of exhumation, i.e. the D2 and D3 phases, were acquired as result of continuous shortening that affected the orogenic wedge during the intraoceanic subduction up to the inception of continental collision. In this picture, only the last D4 phase show structural features referable to extensional tectonics. The complexity of the exhumation path, as also reconstructed for the Lento unit, is also reported by studies about others fossil accretionary wedges, where different processes, as, for instance, a combinations of upward extrusion, extension and erosion [85, 10, 86, 87, 88] have been identified during the exhumation.

Acknowledgements

This research was supported by C.N.R., Istituto di Geoscienze e Georisorse (Pisa) and by M.I.U.R. (PRIN Project). Jacques Malavieille and anonymous referee are also acknowledged for their careful review.

References

[1] Menot, R.P., Orsini, J.B., Évolution du socle anté-stéphanien de Corse: événements magmatique et métamorphiques, Corse. Schweiz. Miner. Petrog. Mitt. 70 (1990) 35-53.

[2] Durand-Delga, M., Principaux traits de la Corse Alpine et correlations avec les Alpes Ligures, Mem. Soc. Geol. It. 28 (1984) 285-329.

[3] Mattauer, M., Proust, F., Etchecopar, A., Linéation "a" et mécanisme de cisellement simple liés au chevauchement de la nappe de schistes lustrée en Corse, Bull. Soc. Géol. Fr. 14 (1977) 841-945.

[4] Faure, M., Malavieille, J., Étude structurale d'un cisaillement ductile: le charriage ophiolitique corse dans la région de Bastia, Bull. Soc. Géol. Fr. 23 (1981) 335-343.

[5] Malavielle, J., Etude tectonique de la nappe de socle de Centuri (zone de schistes lustrés de Corse); conséquences pour la géometrie de la chaine alpine, Bull. Soc. Géol. Fr. 25 (1983) 195-204.

[6] Harris, L., Progressive and polyphase deformation of the Schistes Lustrés in Cap Corse, Alpine Corsica, J. Struct. Geol. 7 (1985) 637-650.

[7] Harris, L., Direction changes in thrusting of the Schistes Lustrés in Alpine Corsica, Tectonophysics 120 (18985) 37-56.

[8] Warburton, J., The ophiolite-bearing Schistes Lustrés nappe in Alpine Corsica: a model for the implacement of ophiolites that have suffered HP/LT metamorphism. Geol. Soc. of Am. Mem 164 (1986) 313-331.

[9] Egal, E., Structures and tectonic evolution of the external zone of Alpine Corsica, J. Struct. Geol. 14 (1992) 1215-1228.

[10] Malavieille, J., Chemenda, A., Larroque, C., Evolutionary model for the Alpine Corsica: mechanism for ophiolite emplacement and exhumation of high-pressure rocks, Terra Nova 10 (1998) 317-322.

[11] Mattauer, M., Proust, F., Données nouvelles sur l'evolution structurale de la Corse alpine, C. R. Acad. Sci. Paris 281 (1975) 1681-1684.

[12] Fournier, M., Jolivet, L., Goffé, B., Dubois, R., The Alpine Corsica metamorphic core complex, Tectonics 10 (1991) 1173-1186.

[13] Jolivet, L., Daniel, J.M., Fournier, M., Geometry and Kinematics of ductile extension in Alpine Corsica, Earth. Planet. Sci. Lett. 104 (1991) 278-291.

[14] Maluski, H., Application de la métode 40Ar/39Ar aux minéraux des roches cristallines perturbées par des événements thermiques et tectoniques en Corse, Thése Doct. Etat, Université Montpellier II, France, (1977) 113 p.

[15] Lahondere, D., Guerrot, C., Datation Sm-Nd du métamorphisme éclogitique en Corse alpine: un argument pour l'existence au Crétacé supérieur d'une zone de subduction active localisée sous le bloc corso-sarde, Géol. France 3 (1997) 3-11.

[16] Caron, J.M., Pequignot, G., The transition between blueschists and lawsonite-bearing eclogites on the example of Corsican metabasalts, Lithos 19 (1986) 205-218.

[17] Lahondere, D., Les schistes bleus et les éclogites à lawsonite des unités continentales et océaniques de la Corse alpine: Nouvelles données pétrologiques et structurales, Thèse de 3ème cycle. Université Montpellier II, France, 1991.

[18] Jolivet, L., Faccenna, C., Goffé, B., Mattei, M., Rossetti, F., Brunet, C., Storti, F., Funiciello, R., Cadet, J.P., Parra, T., Mid-crustal shear zones in post-orogenic extension: the northern Tyrrhenian Sea case, J. Geophys. Res. 103 (1998) 12123-12160.

[19] Brunet, C., Monié, P., Jolivet, L., Cadet, J.P., Migration of compression and extension in the Thyrrenian Sea, insights from 40Ar/39Ar ages on micas along a transect from Corsica to Tuscany, Tectonophysics 321 (2000) 127-155.

[20] Daniel, J.M., Jolivet, L., Goffé, B., Ponssot, C., Crustal-scale strain partitioning: footwall deformation below the Alpine Oligo-Miocene detachment of Corsica, J. Struct. Geol. 18 (1996) 41-49.

[21] Amaudric du Chaffault, S., Kienast, J.R., Saliot, P., Répartition de quelques minéraux du métamorphisme alpin en Corse, Bull. Soc. Géol. Fr. 7 (1976) 149-154.

[22] Amaudric du Chaffault, S., Saliot, P., La région de Corte: sectèur-clè pour la comprèhension du mètamorphisme alpine en Corse, Bull. Soc. Géol. Fr. 21 (1979) 149-154.

[23] Gibbons, W., Horak, J., Alpine metamorphism of Hercynian horneblende granodiorite beneath the Schistes Lustrés nappe of NE Corsica, J. Metam. Geol. 2 (1984) 95-113.

[24] Bezert, P., Caby, R., Sur l'âge post-bartonien des évenements tectono-metamorphiques alpins en bordure orientale de la Corse cristalline (Nord de Corte), Bull. Soc. Géol. Fr. 8 (1988) 965-971.

[25] Molli, G., Tribuzio, R., Shear zones and metamorphic signature of subducted continental crust as tracers of the evolution of the Corsica/Northern Apennine orogenic system, in: Alsop, G.I., Holdsworth, R.E., McCaffrey, K.J.W., Hand M. (Eds.), Flow Processes in Faults and Shear Zones, Geol. Soc. London, Spec. Pub. 224 (2004) pp. 321–335.

[26] Malasoma, A., Marroni, M., Musumeci, G., Pandolfi, L., High-pressure mineral assemblage in granitic rocks from continental units, Alpine Corsica, France, Geol. J. 41 (2006) 49-59.

[27] Marroni, M., Pandolfi, L., Deformation history of the ophiolite sequence from the Balagne Nappe, northern Corsica: insights in the tectonic evolution of Alpine Corsica, Geol. J. 38 (2003) 67-83.

[28] Maluski, H., Mattauer, M., Matte, P., Sur la presence de decrochements alpins en Corse, C. R. Acad. Sci. Paris 276 (1973) 709-712.

[29] Waters, C.N., The Cenozoic evolution of Alpine Corsica, J. Geol. Soc. London 147 (1990) 811-824.

[30] Lacombe, O., Jolivet, L., Structural and kinematic relationship between Corsica and the Pyrenees-Provence domain at the time of the Pyrenean orogeny, Tectonics 24 (2006) TC1003, doi:10.1029/2004TC001673.

[31] Rossi, P., Durand-Delga, M., Lahondere, J.C., Et Coll. (Baud, J.P., Egal, E., Lahondere, D., Laporte, D., Lluch, D., Loyle, M.D., Ohnenstetter, M., Palagi, P., Carte Géologique de France (1/50 000), feuille Santo-Pietro-di-Tenda (1106). Orleans BRGM. Notice explicative par Rossi, P., Durand-Delga, M., Lahondere, J.C., Lahondere, D., 2001, 224 p.

[32] Lahondere, D., Caby, R., Les Meta-conglomerats polygeniques des 'Schistes lustres' de la vallee du Golo (Corse alpine); signification paleogeographique et consequences tectoniques, C. R. Acad. Sci. Paris 309 (1989) 727-732.

[33] Rossi, P., Durand-Delga, M., Caron, J.M., Guieu, G., Conchon, O., Libourel, G., Loye-Pilot, M.D., Olle, J.J., Pequignot, G., Potdevin, J.L., Rieuf, M., Rodriguez, G., Sedan, O., Vellutini, P.J., Rouire, J., 1994a. Carte géologique de la France (1/50 000), feuille Corte (1110). Orléans, BRGM. Notice explicative par Rossi, P., Durand-Delga, M., Caron, J.M., Guieu, G., Conchon, O., Libourel, G., Loye-Pilot, M.D., 1994, 150p.

[34] Ohnestetter, D., Ohnestetter, M., Modèle de fonctionnement d'une ride médio-océanique à partir de l'étude pétrologique des ophiolites corses, Bull. Soc. Géol. Fr. 7 (1976) 889-894.

[35] Decandia, F.A., Elter, P., La zona ofiolitifera del Bracco nel settore compreso tra Levanto e la Val Graveglia (Appennino Ligure), Mem. Soc. Geol. It. 11 (1972) 503-530.

[36] Lagabrielle, Y., Ophiolites of the southwestern Alps and the structure of the Tethyan oceanic lithosphere, Ofioliti 19 (1994) 413-434.

[37] Burroni, A., Levi, N., Marroni, M., Pandolfi, L., Lithostratigraphy and structure of the Lago Nero Unit (Chenaillet Massif, Western Alps); comparison with internal Liguride units of Northern Apennines, Ofioliti 28 (2003) 1-11.

[38] Marroni, M., Monechi, S., Perilli, N., Principi, G., Treves, B., Cretaceous flysch deposits of the Northern Apennines, Italy: age of

inception of orogenesis-controlled sedimentation, Cretac. Res. 13 (1992) 487-504.

[39] Padoa, E., Les ophiolites du massif de l'Inzecca (Corse alpine): litostratigraphie, structure géologique et évolution géodynamique, Géologie de la France 3 (1999) 37- 48.

[40] Ramsay, JG., Folding and fracturing of rocks. Mc Graw, Hill New York, 1967, 568 p.

[41] Passchier, C.W., Trouw, R.A.J., Micro–tectonics. Springer Eds Berlin, 1998, 289 p.

[42] Leake, B.E., Wooley, A.R., Arps, C.E.S., Birch, W.D., Gilbert, M.C., Grice, J.D., Hawthorne, F.C., Kato, A., Kisch, H.J., Krivivichev, V.G., Linthout, K., Laird, J., Mandarino, J.A., Maresch, W.V., Nickel, E.H., Rock, N.M.S., Schumacher, J.C., Smith, D.C., Stephenson, N.C.N., Ungaretti, L., Whittaker, E., Youzhi, G., Nomenclature of Amphiboles. Report of the subcommittee on amphiboles of the International Mineralogical Association Commission on New Minerals and Mineral Names, Mineral. Mag. 61 (1997) 259–321.

[43] Tribuzio, R., Giacomini, F., Blueschist facies metamorphism of peralkaline rhyolites from Tenda crystalline massif (northern Corsica): evidence for involvement in the Alpine subduction event?, J. Metamorph. Geol. 20 (2002) 513-526.

[44] Brown, E.H., The crossite content of Ca-amphibole as a guide to pressure of metamorphism, J. Petrol. 18 (1977) 53-72.

[45] Banno, S., Sakai, C., Geology and metamorphic evolution of the Sambagawa metamorphic belt, Japan, in: Daly, J.S., Cliff, R.A., Yardley, B.W.D. (Eds.), Evolution of Metamorphic Belts, Geol. Soc. London, Spec. Pub. 43 (1989) 519-532.

[46] Evans, B.W., Phase relations in epidote–blueschists, Lithos 25 (1990) 3–23.

[47] Otsuki, M., Banno, S., Prograde and retrograde metamorphism of hematite-bearing basic schists in the Sambagawa belt in central Shikoku, J. Metamorph. Geol. 8 (1990) 425-439.

[48] Liou, J.G., Maruyama, S., Cho, M., Very low-grade metamorphism of volcanic and volcaniclastic rocks–mineral assemblages and mineral facies. In: Frey, M. (Eds.), Low Temperature Metamorphism. Blackie and Son Ltd, Glasgow, 1987, pp. 59-113.

[49] Velde, B., Phengitic micas: Synthesis, stability, and natural occurrence, Am. J. Sci. 263 (1965) 886-913.

[50] Cathelineau, M., Nieva, D., A chlorite solid solution geothermometer. The Los Azufres (Mexico) geothermal system, Contrib. Mineral. Petrol. 91 (1985) 235-244.

[51] Massonne, H.J., Schreyer, W., Phengite geobarometry based on the limitino assemblage with K-felspar, phlogopite, and quartz, Contrib. Mineral. Petrol. 96 (1987) 212-224.

[52] Hillier, S., Velde, B., Octahedral occupancy and the chemical composition of diagenetic (low-temperature) chlorites, Clay Min. 26 (1991) 146-168.

[53] Massonne, H.J., Szpurska, Z., Thermodynamic properties of white micas on the basis of high-pressure experiments in the systems K2O-MgO-Al2O3-SiO2-H2O and K2O-FeO-Al2O3-SiO2-H2O, Lithos 41 (1997) 229-250.

[54] Vidal, O., Parra, T., Trotet, F., A thermodynamic model for Fe-Mg aluminous chlorite using data from phase equilibrium experiments and natural pelitic assemblages in the 100-600°C, 1-25 kbar P-T range, Am. J. Sci. 301 (2001) 557-592.

[55] Vidal, O., Parra, T., Exhumation paths of high-pressure metapelites obtained from local equilibria for chlorite-phengite assemblages, Geol. J. 35 (2000) 139-161.

[56] Parra, T., Vidal, O., Agard, P., A thermodynamic model for Fe-Mg dioctahedral K white micas using data from phase-equilibrium experiments and natural pelitic assemblages, Contrib. Mineral. Petrol. 143 (2002) 706-732.

[57] Berman, R.G., Thermobarometry using multiequilibrium calculations: a new technique with petrologic applications, Can. Mineral. 29 (1991) 833-855.

[58] Berman, R.G., Internally-consistent thermodynamic data for stoichiometric minerals in the system Na2O-K2O-CaO-MgO-FeO-Fe2O3-Al2O3-SiO2-TiO2-H2O-CO2, J. Petrol. 29 (1998) 445-522.

[59] Berman, R.G., Mixing properties of Ca-Mg-Fe-Mn garnets, Am. Miner. 75 (1990) 328-344.

[60] Boccaletti, M., Elter, P., Guazzone, G., Plate tectonic models for the development of the western Alps and Northern Apennines, Nature Physical Sci. 234 (1971) 108-111.

[61] Treves, B., Orogenic belts as accretionary prisms; the example of the Northern Apennines, Ofioliti 9 (1984) 577-618.

[62] Polino, R., Dal Piaz, G.V., Gosso, G., Tectonic erosion at the Adria margin and accretionary processes for the Cretaceous orogeny of the Alps, Mem. Soc. Géol. Fr. 156 (1990) 345-367.

[63] Sample J.C. and Fisher D.M., Duplexes and underplating in an ancient accretionary complex, Kodiak islands, Alaska, Geology, 14 (1986) 160-173.

[64] Sample, J.C., Moore, J.C., Structural style and kinematics of an underplated slate belt, Kodiak and adjacent islands, Alaska, Geol. Soc. Am. Bull. 99 (1987) 7-20.

[65] Cloos, M., Shreve, R.L., Subduction-channel model of wedge accretion, melange formation, sediment subduction, and subduction erosion at convergent plate margins: I. Background and description, Pure Appl. Geophys. (PAGEOPH) 128 (1988) 455-500.

[66] Kimura, G., Maruyama, S., Isozaki, Y., Terabayashi, M., Well-preserved underplating structure of the jadeitized Franciscan complex, Pacheco Pass, California, Geology 24 (1996) 75-78.

[67] Marroni, M., Pandolfi, L., Meneghini, F., From accretion to exhumation in a fossil accretionary wedge: a case history from Gottero Unit (Northern Apennines, Italy), Geodin. Acta 17 (2004) 41-53.

[68] Fisher, D.M., Byrne, T., Structural evolution of underthrusted sediments, Kodiak Islands, Alaska, Tectonics 6 (1987) 775-793.

[69] Kimura, G., Mukai, A., Underplated units in an accretionary complex-melange of the Shimanto Belt of eastern Shikoku, southwest Japan, Tectonics 10 (1991) 31-50.

[70] Willett, S.D., Dynamic and kinematic growth and change of a Coulomb wedge. In: McClay, K.R. (Eds.), Thrust tectonics, Chapman and Hall, London, 1992, pp. 19-31.

[71] Glodny, J., Lohrmann, J., Echtler, H., Grafe, K., Seifert, W., Collao, S., Figueroa, O., Internal dynamics of a paleoaccretionary wedge: insights from combined isotope tectonochronology and sandbox modeling of the South-Central Chilean forearc, Earth Planet. Sci. Lett. 231 (2005) 23-39.

[72] Mattauer, M., Faure, M., Malavieille, J., Transverse lineation and large-scale structures related to Alpine obduction in Corsica, J. Struct. Geol. 3 (1981) 401-409.

[73] Caron, J.M., Metamorphism and deformation in Alpine Corsica, Schweiz. Miner. Petrog. Mitt. 74 (1994) 105-114.

[74] Platt, J.P., Mechanics of oblique convergence, J. Geophys. Res. 98 (1993) 16239-16256.

[75] Martinez, A., Malavieille, J., Lallemand, S., Collot, J.Y., Partition de la deformation dans un prisme d'accrétion sédimentaire en convergence oblique: approcheexpérimentale, Bull. Soc. Géol. Fr. 173 (2002) 17-24.

[76] Konstantinovskaia, E., Malavieille J., Erosion and exhumation in accretionary orogens: Experimental and geological approaches. Geochemistry, Geophysics, Geosystems 6 (2005) Q02006, doi: 10.1029/2004GC000794.

[77] Gutscher, M.A., Kukowski, N., Malavieille, J., Lallemand, S., Episodic imbricate thrusting and underthrusting: analog experiments and mechanical analysis applied to the Alaskan Accretionary Wedge, J. Geophys. Res. 103 (1998) 10161-10176.

[78] Kukowski, N., Lallemand, S.E., Malavieille, J., Gutscher, M.A., Reston, T.J., Mechanical decoupling and basal duplex formation observed in sandbox experiments with application to the Western Mediterranean Ridge accretionary complex, Mar. Geol. 186 (2002) 29-42.

[79] Ratschbacher, L., Frisch, W., Neubauer, F., Schmid, S.M., Neugebauer, J., Extension in compressional orogenic belts: The Eastern Alps, Geology 17 (1989) 404-407.

[80] Frotzheim, N., Formation of recumbent folds during synorogenic crustal extension (Austroalpine nappes, Switzerland), Geology 20 (1992) 923-926.

[81] Wheeler, J., Butler, R.W.H., Criteria for identifying structures related to true extension in orogens, J. Struct. Geol. 16 (1994) 1023-1027.

[82] Marroni, M., Treves, B., Hidden Terranes in the northern Apennines, Italy: a record of Late Cretaceous-Oligocene transpressional tectonics, J. Geol. 106 (1998) 149-162.

[83] Schoonover, M., Osozawa, S., Exhumation process of the Nago subduction-related metamorphic rocks, Okinawa, Ryukyu island arc, Tectonophysics 393 (2004) 221-240.

[84] Ring, U., Reischmann, T., The weak and superfast Cretan detachment, Greece: exhumation at subduction rates in extruding wedges, J. Geol. Soc. London 159 (2002) 225-228.

[85] Hacker, B.R., Ratschbacher, L., Webb, L., Shuwen, D., What brought them up? Exhumation of the Dabie Shan ultrahighpressure rocks, Geology 23 (1995) 743-746.

[86] Burov, E., Jolivet, L., Le Pourhiet, L., Poliakov, A., A thermomechanical model of exhumation of high pressure (HP) and ultra-high pressure (UHP) metamorphic rocks in Alpine-type collision belts, Tectonophysics 342 (2001) 113-136.

[87] Lin, C.H., Active continental subduction and crustal exhumation: the Taiwan orogeny, Terra Nova 14 (2002) 281-287.

[88] Froitzheim, N., Pleuger, J., Roller, S., Nagel, T., Exhumation of high- and ultrahigh-pressure metamorphic rocks by slab extraction, Geology 31 (2003) 925– 928.